WILEY

Cladistics

Cladistics 42 (2026) 172–192

doi: 10.1111/cla.70019

A new Chinese dicynodont and the frequent dispersal of tetrapods between Northern and Southern Pangaea during the late Permian

Yu-Tai Shi[a,b,*] and Jun Liu[a,b,*]

[a]*Key Laboratory of Vertebrate Evolution and Human Origins, Institute of Vertebrate Paleontology and Paleoanthropology, Chinese Academy of Sciences, Beijing, China;* [b]*College of Earth and Planetary Sciences, University of Chinese Academy of Sciences, Beijing, China*

Received 18 May 2025; Revised 14 October 2025; Accepted 22 October 2025

Abstract

The dispersal pattern of tetrapods across Pangaea is a crucial problem for understanding Permian terrestrial ecosystems. This study describes a rare cross-equatorial record of a dicynodont genus. New fossil material from China can be referred to *Dinanomodon*, a genus formerly only known from South Africa, although it represents a new species—*D. guoi*. To investigate the divergence of Bidentalia, a newly assembled dataset was employed to perform maximum parsimony analysis, Bayesian inference and the first tip-dating analysis within the anomodonts. Considering other tetrapod occurrences, we suggest that frequent cross-equatorial dispersal of tetrapods occurred during the Lopingian (late Permian). Based on tetrapod distribution and paleoclimate data, precipitation, rather than temperature, probably represents the major ecological factor influencing corridors for dispersal along the eastern margin of Pangaea.

Introduction

The formation of Pangaea in the late Palaeozoic represents one of the most significant tectonic events in Earth's history (Klein, 1994). New fossil evidence indicates that the assembly of the North China Block into Pangaea could have occurred as early as the Cisuralian (early Permian) (Chen and Liu, 2024). Although the supercontinent enabled global dispersal of terrestrial tetrapods, shared low-rank taxonomic records between the Laurasian and Gondwanan faunas remain rare, even during the Lopingian (late Permian) (Liu and Abdala, 2022). This indicates that some barriers to dispersal remained even on a contiguous land mass.

Dicynodonts, the most diverse Permian tetrapods, have been collected on all continents (King, 1988; Fröbisch, 2009). However, even in this versatile clade, there are very few records of shared genera between Laurasia and Gondwana (i.e. Northern and Southern Pangaea). Only in the genera *Diictodon*, *Geikia*, and possibly *Lystrosaurus* is there evidence for cross-equatorial distribution during the Lopingian (Yuan and Young, 1934; Rowe, 1980; Angielczyk and Sullivan, 2008). (The age of the Laurasian *Lystrosaurus* records is uncertain; no conclusive Permian *Lystrosaurus* records in Laurasia are currently known; Surkov et al., 2005; Angielczyk et al., 2022.)

Dinanomodon is a large Permian dicynodont, at present considered a monotypic genus. Like many dicynodonts, it has a complex taxonomic history. Broom (1932, p. 176) described a poorly preserved skull (SAM-PK-4008) from the '*Cistecephalus* zone' of Graaff-Reinet, South Africa, and noted that 'the median process of the premaxilla meets the frontals'. Based on this unique character, he named it *Dicynodon gilli*. Later, Broom (1938, p. 247) established the genus *Dinanomodon* based on the type species *Din. rubidgei* (holotype RC 9) from Graaff-Reinet, which was characterized by a sharply pointed premaxilla 'like the beak of a huge bird of prey'. In 1940, Broom named

*Corresponding author:
E-mail address: shiyutai@ivpp.ac.cn (Y.-T.S.); liujun@ivpp.ac.cn (J.L.)
urn:lsid:zoobank.org:pub:0DF9EC82-66D4-46A4-B534-AC074F54C04

additional species of *Dicynodon* and *Dinanomodon*: *Dic. anneae* (Broom, 1940a), *Dic. macrodon* (Broom, 1940b) and *Din. gigas* (Broom, 1940a). Broom and Robinson (1948, p. 406) described a 'remarkably aberrant' *Dicynodon* species that they named *Dic. galecephalus*. These species underwent numerous revisions in the second half of the 20th century (see details in Kammerer et al. (2011)). Kitching (1977) proposed *Din. gigas* as a junior synonym of *Din. rubidgei*. Keyser and Cruickshank (1979) accepted *Dinanomodon* as a valid genus and suggested that *Kannemeyeria* descended from it. Cluver and King (1983) proposed that *Dinanomodon* be treated as a synonym of *Dicynodon* and considered it closely related if not identical to *Dic. leoniceps*. However, King (1988) later followed the views of Keyser and Cruickshank (1979) and accepted *Din. gigas* as a valid species. Kammerer et al. (2011) conducted a comprehensive taxonomic revision of the nominal species of *Dicynodon*. Their results further validated *Dinanomodon* as a distinct genus and they considered the type specimens of *Dic. gilli*, *Dic. anneae*, *Dic. macrodon*, *Dic. galecephalus*, *Din. rubidgei* and *Din. gigas* to belong to it. Based on the principle of priority, they affirmed *Dinanomodon gilli* as the only valid specific name for this genus.

In 2020, some late Permian tetrapod fossils were discovered in Jingtai County and Gulang County (Gansu Province) during an expedition led by Drs. Li Da-Qing and Yi Hong-Yu. In subsequent years, numerous tetrapod fossils were collected from this region, from where *Moschowhaitsia lidaqingi*, a large carnivorous therocephalian, was the first tetrapod reported (Liu and Abdala, 2023). Here we establish a new species of *Dinanomodon* based on a skull from the initial expedition, demonstrating that *Dinanomodon* exhibited a cross-equatorial distribution during the Lopingian.

Institutional abbreviations

CGS, Council for Geoscience, Pretoria, South Africa; IVPP, Institute of Vertebrate Palaeontology and Paleoanthropology, Chinese Academy of Sciences, Beijing, China; NMQR, National Museum, Bloemfontein, South Africa; RC, Karoo Origins Centre (Rubidge Collection), Graaff-Reinet, South Africa; SAM, Iziko South African Museum, Cape Town, South Africa.

Materials and methods

The new Chinese dicynodont specimen (IVPP V31930) consists of a complete skull with a basal length of 273 mm. Only the anterior snout surface is eroded. (Figs 1–3).

Comparative South African specimens: CGS AK82-7, NMQR 77, RC 9, RC 22, SAM-PK-4008, SAM-PK-K10220, SAM-PK-K10618 (Figs 4 and 5).

Phylogenetic analysis

A dataset of non-kannemeyeriiform dicynodonts, which contained 99 operational taxonomic units (OTUs) and 213 characters, was compiled from previous studies (Liu, 2022; Macungo et al., 2022; Angielczyk et al., 2023; Shi and Liu, 2023; Shi and Liu, 2024; George et al., 2025). '*Eodicynodon*' *oelofseni* was renamed *Nyaphulia oelofseni* following Duhamel et al. (2024), while *Endothiodon mahalanobisi* was added and coded based on Ray (2000) and Maharaj et al. (2024). 'Shansiodontids', *Dinodontosaurus tener*, *Sinokannemeyeria*, *Shaanbeikannemeyeria xilougouensis* and *Ischigualastia jenseni* represented kannemeyeriiforms. *Biarmosuchus tener* was used as the outgroup in all analyses to root the trees.

The utility of continuous characters in phylogenetics remains debated (Pimentel and Riggins, 1987; Felsenstein, 1988; Rae, 1998; Goloboff et al., 2006; Hendrixson and Bond, 2009; Bardin et al., 2014; Holvast et al., 2024; Saguir et al., 2025; Tagliacollo et al., 2025). With regard to dicynodonts, the continuous characters resulted in apparently fully resolved topologies with low support values and high topological instability (Angielczyk and Kammerer, 2017; Kammerer and Ordoñez, 2021). In this analysis, the character list and codings were completely revised, unconstitutive discrete-state characters for OTUs were deleted, three characters from the epipterygoid (Ch. 196–198) were added (Supporting Information), and several miscodings were corrected. The continuous character data were discretized via homogeneous-subset coding proposed by Simon (1983) and modified by Archie (1985). This method adopts the Tukey–Kramer test to assess the significance between two differences in continuous codings. Those OTUs with significant differences are assigned to distinct states; otherwise, they receive an identical state. Those single-specimen OTUs were assigned based on the OTUs with the closest mean values. The agricolae package in R (de Mendiburu, 2023; R Core Team, 2024) was used to implement this workflow. Because the tip-dating analysis limits ordered characters to six states, the data were manually merged subsequently. Finally, fifteen discretized continuous characters (Ch. 199–213) were reintroduced (Supporting Information).

The characters 12, 34, 58, 61, 78, 138, 148, 149, 164, 173, 199–213 were treated as ordered.

Parsimony analysis

TNT version 1.6 (Goloboff and Morales, 2023) was employed to perform the parsimony analysis. First, the New Technology search was used with the initial search level set to 65, which was checked every 3 hits. The initial number of addition sequence replicates was 1000, and the search was forced to find the minimum length at least 50 times. The analysis employed sectorial searching, tree drifting, parsimony ratchet and tree fusing for searching. Subsequently, the Traditional search was used to analyse the trees from the memory. Bremer support values were utilized to evaluate clade support. These values were based on 100 000 suboptimal trees with length up to 6 steps longer than the most parsimonious trees. Wincladtree script for TNT (Goloboff, 2024) was additionally used to output the synapomorphies (Fig. S1).

Bayesian inference

MrBayes v3.2.7 (Ronquist et al., 2012) was employed to perform the non-calibrated analysis; the MkV model (Lewis, 2001) was adopted as the substitution model. Two runs were set, each with four chains and 250 000 000 generations, with sampling every 25 000 generations. The first 25% of sampled trees were discarded as burn-in. The average standard deviation of split frequencies (ASDSF) was <0.01. The effective sample size (ESS >200) and

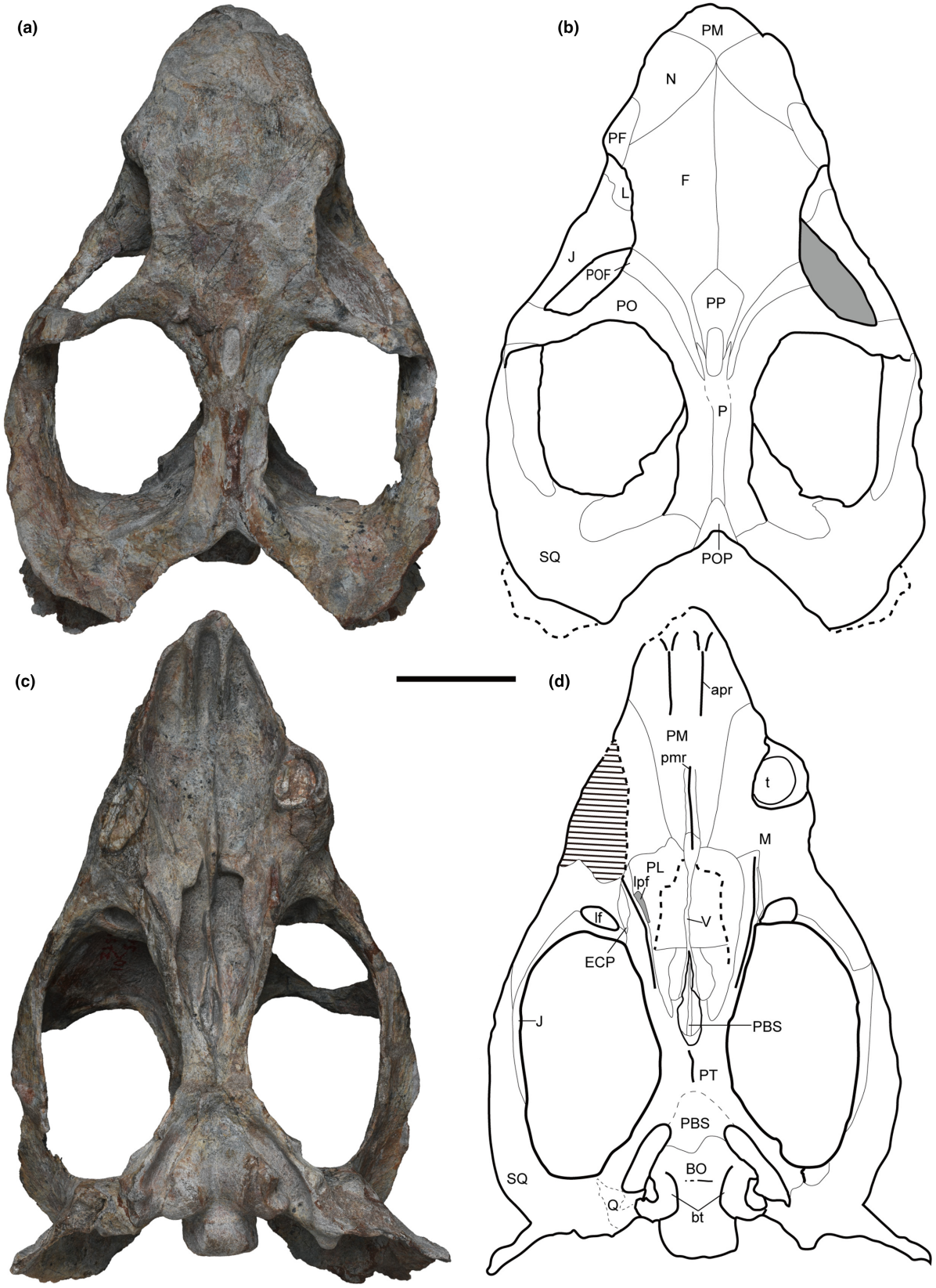

Fig 1. Photos and drawings of *Dinanomodon guoi* (IVPP V31930) in (a, b) dorsal and (c, d) ventral views. apr, anterior palatal ridge; BO, basioccipital; bt, basal tuber; ECP, ectopterygoid; F, frontal; J, jugal; L, lacrimal; lf, labial fossa; lpf, lateral palatal foramen; M, maxilla; N, nasal; P, parietal; PBS, parabasisphenoid; PF, prefrontal; PL, palatine; PM, premaxilla; pmr, posterior median ridge; PO, postorbital; POF, postfrontal; POP, postparietal; PP, preparietal; PT, pterygoid; Q, quadrate; SQ, squamosal; t, tusk; V, vomer. Scale bar equal 5 cm.

parameter convergence were assessed using Tracer v1.7.2 (Rambaut et al., 2018).

Tip-dating analyses

The tip-dating analyses were also performed on MrBayes v3.2.7, with the MkV model again serving as the substitution model. The clock rate prior used the exponential function, and the parameter was estimated using the non-calibrated Bayesian tree. The white noise model (IGR of MrBayes v3.2.7) was used for the relaxed morphology clock. The fossilized birth–death (FBD) model was used for the tree prior (Stadler, 2010). Because tip-dating analysis requires at least one living taxon, the youngest taxon in our dataset—the Late Triassic *Ischigualastia jenseni*—was designated as the 'living' taxon. All ages of taxa were subtracted 230 Ma (a depositional age from the Ischigualasto Formation (Colombi et al., 2021)). Accordingly, a low living sampling probability (0.0001) was adopted, and diversified sampling was implemented (Zhang et al., 2016). The speciation rate prior used an exponential function (exp (100)), while the extinction rate prior and fossil discovery rate prior used a beta function (beta (1,1)).

The uniform distributions were assigned to the terminal taxon ages, with the exception of *Ischigualastia jenseni*, which was fixed at 0 Ma. Given the high-resolution Permian–Triassic chronostratigraphic framework established in the Karoo Basin of South Africa and the Turpan-Hami and Junggar basins of China, absolute time intervals were used for age distributions. The taxon ranges and ages were obtained from Rubidge et al. (2013), Day et al. (2015), Day and Rubidge (2020), Day and Smith (2020), Gastaldo et al. (2020), Smith et al. (2020) and Viglietti (2020) for South African taxa, Sennikov and Golubev (2017) and Davydov et al. (2020) for Russian taxa, Yang et al. (2021) for some Chinese taxa and Irmis et al. (2022) for South American taxa. Taxa from those horizons without radioisotopic age constraints were assigned to broad ranges (i.e. late Permian) to avoid prior bias. The root age prior was assigned to an offset exponential distribution. Two runs were performed, each with four chains and 600 000 000 generations. Sampling frequency was every 25 000 generations.

After the initial analysis under those parameters, the divergence times of Kingoriidae, *Emydops*, *Endothiodon*, *Dinanomodon*, Rhachiocephalidae and some geikiids were younger than their first appearance datum (FAD) (Fig. S2). Thus, some constraints were added to calibrate these nodes. The node age priors were assigned to an offset exponential distribution. Other procedures matched those of the non-calibrated Bayesian inference.

Results

Systematic palaeontology

Anomodontia Owen, 1860
Dicynodontia Owen, 1859
Bidentalia Bain vide Owen, 1876
Dicynodontoidea Olson, 1944
Dinanomodon Broom, 1938

Type species. *Dinanomodon rubidgei* Broom, 1938 (currently considered synonymous with *Dinanomodon gilli* (Broom, 1932); see Kammerer et al., 2011).

Revised diagnosis. Large Permian dicynodontoid with a low cranium; notch on dorsal edge of nares present; erupted portion of tusk anterior to orbital; lowered posterior section of palatine with anterior section flush with secondary palate; lacrimal swollen; postparietal half-surrounded by supraoccipital. Distinguished from all other Permian dicynodonts by sharply pointed and strongly hook-like snout tip. Distinguished from all dicynodontoids other than *Turfanodon* by contact between premaxilla and frontal. Distinguished from *Turfanodon* by absence of converging ventral ridges on posterior portion of anterior pterygoid rami. Distinguished from all dicynodontoids other than *Jimusaria* by nasal bosses above external nares giving nares a 'saddle-shaped' appearance in lateral view.

Dinanomodon guoi sp. nov.
https://zoobank.org/E66052D6-A5FC-4C14-B14F-5A1241968C75

Etymology. Dedicated to Mr Guo Wan-Gang, the forestry hero and Babusha Forest Farm director, who is also from Gulang County. He represents the second generation of the 'Six Old Men' who fought desertification along the southern edge of the Tengger Desert, making a significant contribution to stopping its expansion.

Holotype. IVPP V31930, a complete cranium.

Type locality and horizon. Shijingzi Village, Xinbu Township, Gulang County, Gansu Province, China. Putative Sunan Formation, upper Permian.

Diagnosis. Distinguished from its congener *Din. gilli* by absence of caniniform buttress; lateral margin of subtemporal bar ventrally deflected; small postparietal contribution to intertemporal bar; lacrimal boss confluent with prefrontal boss.

Description

The fused premaxilla shows a special shape among the dicynodonts. The anterior tip of the premaxilla forms a sharp beak (Fig. 1), similar to that of *Din. gilli* (Fig. 5f,g). *Keyseria* also possesses a triangular premaxilla, but with a blunter anterior tip compared to *Dinanomodon* (Kammerer et al., 2011). The anterior tip of the premaxilla is oriented anteroventrally and hook-like, with the paired anterior palatal ridges also exposed in lateral view (Fig. 2a,b). The posterior median ridge is present, without lateral depressions or ridges (Fig. 1c,d).

The length of the snout region is about 26% of the basal length of the skull. Similar to some other dicynodontoids (*Dicynodon*, *Vivaxosaurus*, *Sintocephalus*), IVPP V31930 displays a relatively low height (Fig. 2a).

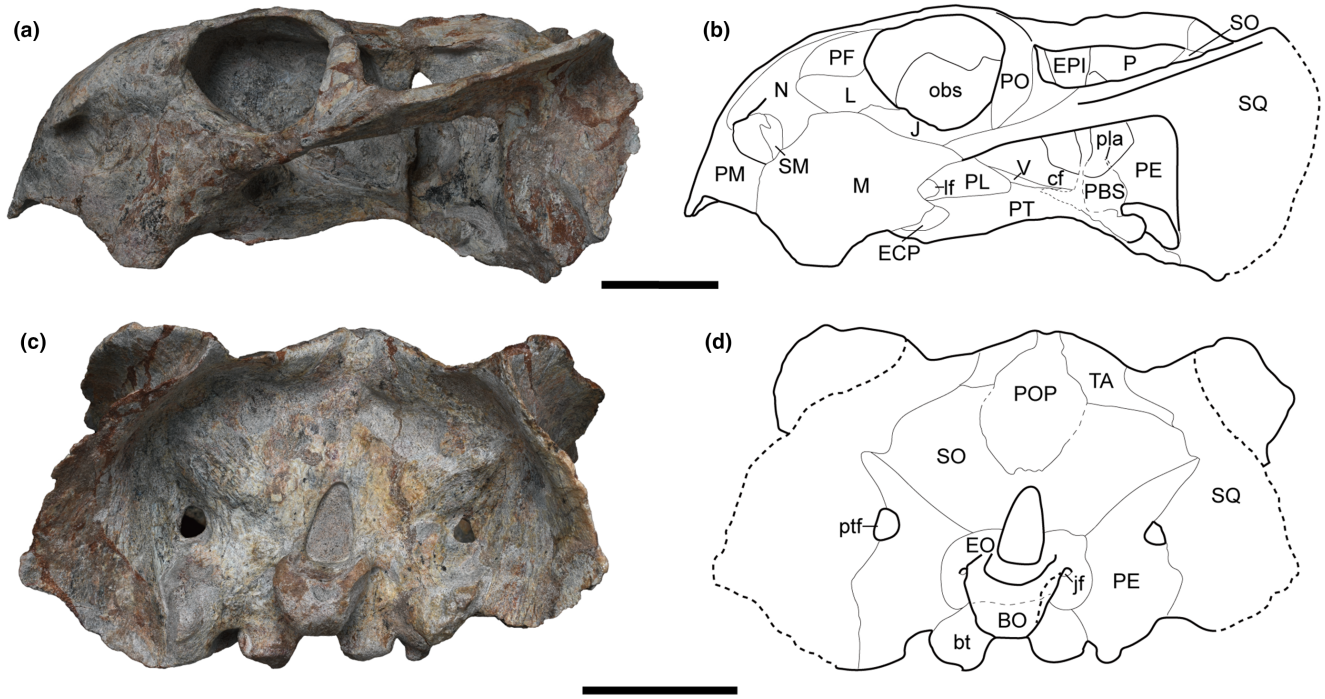

Fig 2. Photos and drawings of *Dinanomodon guoi* (IVPP V31930) in (a, b) lateral and (c, d) occipital views. BO, basioccipital; bt, basal tuber; cf, cultriform process; EC, ectopterygoid; EO, exoccipital; EPI, epipterygoid; F, frontal; J, jugal; jf, jugular foramen; L, lacrimal; la, lacrimal fossa; lf, labial fossa; M, maxilla; N, nasal; obs, orbital septum; P, parietal; PBS, parabasisphenoid; PE, periotic; PF, prefrontal; PL, palatine; pla, pila antotica; PM, premaxilla; PO, postorbital; POP, postparietal; PT, pterygoid; ptf, post-temporal fenestra; SM, septomaxilla; SO, supraoccipital; SQ, squamosal; TA, tabular; V, vomer. Scale bars equal 5 cm.

The moderately developed nasal boss and prefrontal boss are distinct from each other (Fig. 2a). These bosses do not form a prominent anterior expansion of the snout region. The nasal boss creates a 'saddle-shaped' dorsal margin of the naris in lateral view (Fig. 2a,b), as in *Din. gilli* (Fig. 5a–d) and *Jimusaria* (Kammerer et al., 2011; Shi and Liu, 2023). Anterior to the nasal boss, the dorsal notch of the naris is positioned at the junction between the premaxilla and the nasal, located in the anterodorsal corner of the naris (Figs 2a and 3). The naris is bordered by the premaxilla anteroventrally, the nasal dorsally, the maxilla posteroventrally and the septomaxilla posteriorly (Figs 2a,b and 3). The septomaxilla is a tiny, plate-like bone that forms the postnarial excavation with the maxilla and the nasal (Fig. 2a, b). This septomaxilla closely resembles that of *Din. gilli* (SAM-PK-K10220), where it develops as a slender element on the posterior wall of the naris. This morphology contrasts with that of *Turfanodon*, *Daptocephalus* and *Dicynodon*, which have relatively large septomaxillae and in which the nasals either do not or only minimally contribute to the posterodorsal portion of the embayment (Ewer, 1961; Kammerer, 2019b; Liu, 2021; Shi and Liu, 2024). *Repelinosaurus*, in turn, has a narrow septomaxilla that neither contacts the nasal nor exhibits the postnarial excavation (Olivier et al., 2019).

Fig 3. Photo of *Dinanomodon guoi* (IVPP V31930) in anterior view. Scale bar equals 5 cm.

The lacrimal forms the anteroventral margin of the orbit, as in most dicynodonts (Fig. 2a,b). The lacrimal is swollen and confluent with the prefrontal boss in the snout region (Fig. 2a). A similar configuration can be observed in *Taoheodon* (Liu, 2020) and adult

Pelanomodon (Kammerer et al., 2015). In contrast, *Din. gilli* has a lacrimal boss separated from the prefrontal boss, a feature shared with *Delectosaurus* (Kurkin, 2001), where the lacrimal boss is less developed (Fig. 5c,d).

The jugal is exposed as a thin strip ventral to the orbit and contributes to the postorbital bar, extending from the zygomatic bar to the subtemporal bar, covering their medial margin (Fig. 2a,b).

The maxilla has a reduced caniniform process, while its ventral end is incomplete, especially on the right side (Fig. 1c). Its lateral surface is relatively smooth, but bulges in the posteroventral alveolar region around the tusk (Fig. 2a). This morphology differs from *Din. gilli*, which has a distinct buttress clearly demarcating the lateral and posterior surfaces (Fig. 5).

The nasal boss, as noted above, expands laterally and forms a continuous, low swelling dorsally (Fig. 1a). In *Din. gilli*, even the largest individuals (basal skull length >50 cm, see Fig. 4 for NMQR 77 and RC 9) show less pronounced nasal bosses than in *Turfanodon* (Liu, 2021; Shi and Liu, 2024) or *Daptocephalus* (Ewer, 1961; Kammerer, 2019b).

The frontal contacts the premaxilla (Fig. 1b), as in *Turfanodon* (Sun, 1973; Li et al., 2000; Liu, 2021; Shi and Liu, 2024). This character results from the distinct anterior extension of the frontals, which is known only in *Dinanomodon* and *Turfanodon*. It differs markedly from the case in *Bulbasaurus*, where the premaxilla nearly contacts the frontals, but as a result of an extremely elongated, stripe-like ascending process of the premaxilla (Kammerer and Smith, 2017).

The frontal region of IVPP V31930 is relatively smooth, with only a ridge along the posterior portion of the frontal median suture (Fig. 1a). No rugosities, ridges or crests are present along the orbital margin or sutures with other bones. In relatively small *Din. gilli* specimens (e.g. RC 22), the frontal shows a raised orbital margin, but this feature is absent in larger specimens (e.g. NMQR 77, RC 9, SAM-PK-K10220) (Fig. 4). A distinct postfrontal bone is identified between the frontal and postorbital.

The preparietal is almost flush with the skull roof (Fig. 1a,b), and its length varies among *Dinanomodon* specimens (Fig. 4). It is surrounded by the frontals and the parietals, forming the anterior margin of the parietal foramen. The narrow intertemporal bar is composed of the postorbital, the parietal and the postparietal (Fig. 1a,b), while the postparietal is excluded from the intertemporal bar in *Din. gilli* (Kammerer et al., 2011). The intertemporal bar in *Dinanomodon* shows a negative allometric growth trajectory, consistent with many bidentalians (Table 1) (Kammerer et al., 2015; Shi and Liu, 2024). IVPP V31930 also has a narrow exposure of the parietal (Fig. 1a,b).

Anteriorly, the postfrontal-frontal suture is partly elevated as a ridge (Fig. 1), as in *Din. gilli*. In the intertemporal bar, the postorbital laterally expands to form a ventral fossa with the parietal, as in other Permian dicynodonts (Fig. 2a). On its dorsal surface, the postorbital contacts the squamosal at the posteromedial corner of the temporal fenestra (Fig. 1a,b). The suture is constrained to the posteromedial corner, without extending along the posterior margin of the squamosal. The postorbital also forms almost the entire postorbital bar, with only the base also contributed by the jugal (Fig. 2a,b). In lateral view, the postorbital ventrally touches the squamosal at a point. *Turfanodon*, *Daptocephalus* and *Delectosaurus* also have a posterior exposure of the jugal on the base of the postorbital bar (Ewer, 1961; Angielczyk and Kurkin, 2003; Kammerer, 2019b; Shi and Liu, 2024), but their jugal exposures are not as large as those of IVPP V31930.

The squamosal extends anteriorly below the middle part of the orbit and contacts the maxilla. Its width expands within the subtemporal bar (Fig. 1c,d). Laterally, the margin is mildly curved ventrally (Fig. 2a), different from *Din. gilli* but similar to some cryptodonts (Kammerer and Smith, 2017). The relative height of the dorsolateral notch, formed by the zygomatic and quadrate rami of the squamosal, is comparable to that of *Daptocephalus* (Ewer, 1961; Kammerer, 2019b) but greater than that of *Turfanodon* and *Dicynodon* (Sun, 1973; Kammerer, 2019b; Kammerer et al., 2022). The quadrate ramus of the squamosal descends vertically and expands anteroposteriorly (Fig. 2a,b). The quadratojugal-quadrate complex is heavily eroded, with only a small portion of the quadrate remaining (Fig. 1c,d).

In ventral view, the secondary palate is mainly formed by the premaxilla, although the maxilla and the palatine also contribute to it (Fig. 1c,d). The vomer extends posteriorly from the end of the posterior median ridge to the anterior margin of the interpterygoid vacuity. The median plate of the vomer is incomplete and shapes the posterior portion of the nasal septum. This sheet-like element bifurcates posteriorly and expands laterally into two plate-like elements, which form the posterior wall of the choanae. This bifurcation forms the anterior half of the margin of the interpterygoid vacuity, and these plate-like elements rise and clasp the parabasisphenoid (Fig. 2a,b).

The palatine is surrounded anteriorly by the premaxilla and maxilla, laterally and posteriorly by the pterygoid and medially by the vomer (Fig. 1c,d). The palatine forms most of the choana wall. Ventrally, it descends from the secondary palate with only the most anterior tip flush with the premaxilla, so the palatine pad is separated into two portions by a groove (Fig. 1c). In *Din. gilli*, the anterior portion, which is flush with the premaxilla, is larger than the posterior portion (Fig. 5f,g).

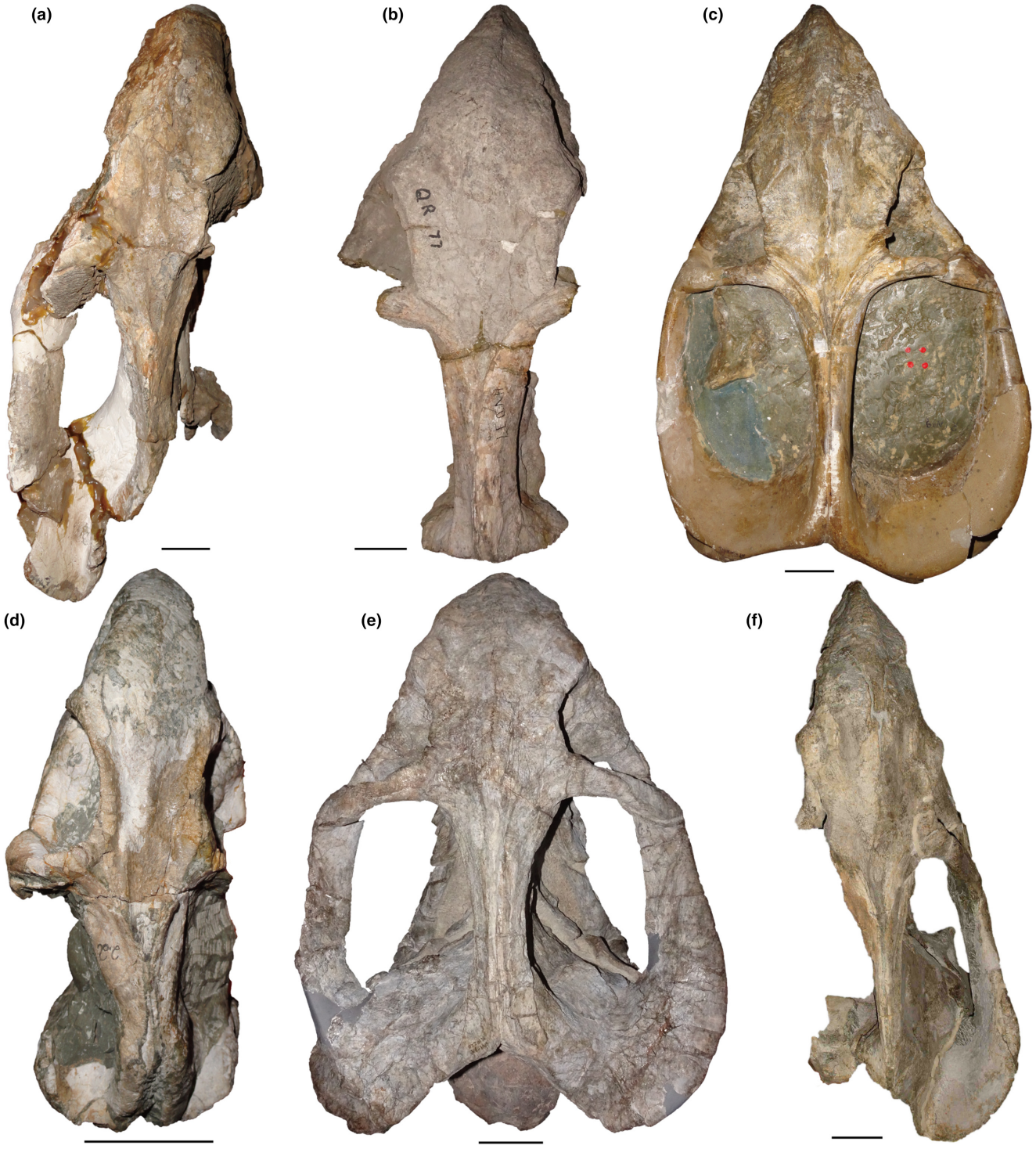

Fig 4. Photos of *Dinanomodon gilli* in dorsal view: (a) CGS AK82-7, (b) NMQR 77, (c) RC 9, (d) RC 22; (e) SAM-PK-K10220; (f) SAM-PK-K10618. Scale bars equal 5 cm.

On both sides, the medial margin of the palatine is eroded, obscuring the shape of the choana. A slender lateral palatal foramen is observed on the right side, between the palatine and the anterior ramus of the pterygoid. Posteriorly, the palatine extends along the medial wall of the anterior ramus of the pterygoid. It also contributes to the margin of the labial fossa with the maxilla and the jugal (Fig. 2a,b).

Table 1
Cranial measurements for *Dinanomodon*

Specimens	Preorbital/basal length	Interorbital/basal length	Intertemporal bar posterior portion/anterior portion	Width of intertemporal bar/basal length	Temporal fenestra/Basal length	Relative position of pineal foramen	Width of median pterygoid plate/basal length	Length of interpterygoid vacuity/basal length	Dorsal skull length/basal length
RC 22	0.246	0.185	0.556	0.134	/	0.333	0.094	/	/
RC 9	0.391	0.193	0.300	0.067	/	0.563	0.119	0.096	1.046
SAM-PK-K10618	0.351	0.241	0.407	0.050	0.619	0.617	0.110	0.110	1.046
SAM-PK-K10220	0.413	0.263	0.579	0.107	0.505	0.832	/	/	/
IVPP V31930	0.267	0.257	0.694	0.114	0.340	0.465	0.100	0.161	0.811

In ventral view, the ectopterygoid extends less posteriorly than the palatine (Figs 1c,d and 2a,b). The pterygoid is a typical X-shaped element (Fig. 1c,d). The lateral expansion of its anterior rami is comparable in scale to that of *Turfanodon* and *Daptocephalus* but narrower than that of *Dicynodon* (Kammerer, 2019b; Liu, 2021). In larger specimens of *Din. gilli* (CGS AK82-7, Fig. 5g), the expansion appears narrower, potentially due to ontogenetic variation, a trend that can also be observed in *Turfanodon* (Liu, 2021; Shi and Liu, 2023). The anterior pterygoid keel runs nearly the entire length of the anterior ramus, converging and gradually decreasing in height posteriorly. The interpterygoid vacuity lies between the anterior rami of the pterygoid and anterior to the median pterygoid plate. The posterior margin of this vacuity is formed by the pterygoid, which extends ventrally to the plate. The parabasisphenoid is visible through this vacuity. A thin median ridge is developed on the median pterygoid plate. The quadrate rami of the pterygoid extend posteriorly to the quadrate, with similar lateral expansion to that of *Turfanodon*, wider than in *Daptocephalus* and narrower than in *Dicynodon*.

Posterior to the median pterygoid plate, the suture is indistinct, but the parabasisphenoid can still be identified (Fig. 1c,d). The parabasisphenoid can be roughly divided into two portions exposed ventrally: a depressed anterior portion and the sloping anterior portions of the basal tubera posteriorly. A similar parabasisphenoid depression is also present in *Turfanodon* (Liu, 2021). The internal carotid canal is not clearly preserved. The sloping portions of the basal tubera bear two blunt ridges that extend from the parabasisphenoid depression to the anterior edges of the basal tubera posteroventrally. The majority of the basal tubera is formed by the basioccipital and these structures appear rounded, although this is due in part to ventral erosion. The intertuberal ridge is partly preserved on the left side, where it appears swollen. In lateral view, the parabasisphenoid extends anteriorly from the periotic as the cultriform process (Fig. 2a,b). Due to the unprepared matrix, the sutures of other sphenoid elements are unclear. The orbital septum ('anterior plate' of dicynodonts) is formed by the orbitosphenoid and the mesethmoid (the sphenethmoid complex), and the lateral wing of the orbitosphenoid contacts the frontal posteriorly (Fig. 2a,b).

The epipterygoid is observed on the left lateral side; only its ascending ramus and quadrate ramus remain (Fig. 2a,b). In *Din. gilli*, the epipterygoid has an anteriorly elongated footplate bearing a dorsal process at its anterior end. Extending from the footplate, the quadrate ramus runs posteriorly, approaching but not contacting the quadrate. This ramus expands into a sheet-like structure that covers the quadrate ramus of the pterygoid (Fig. 2a,b). The ascending ramus

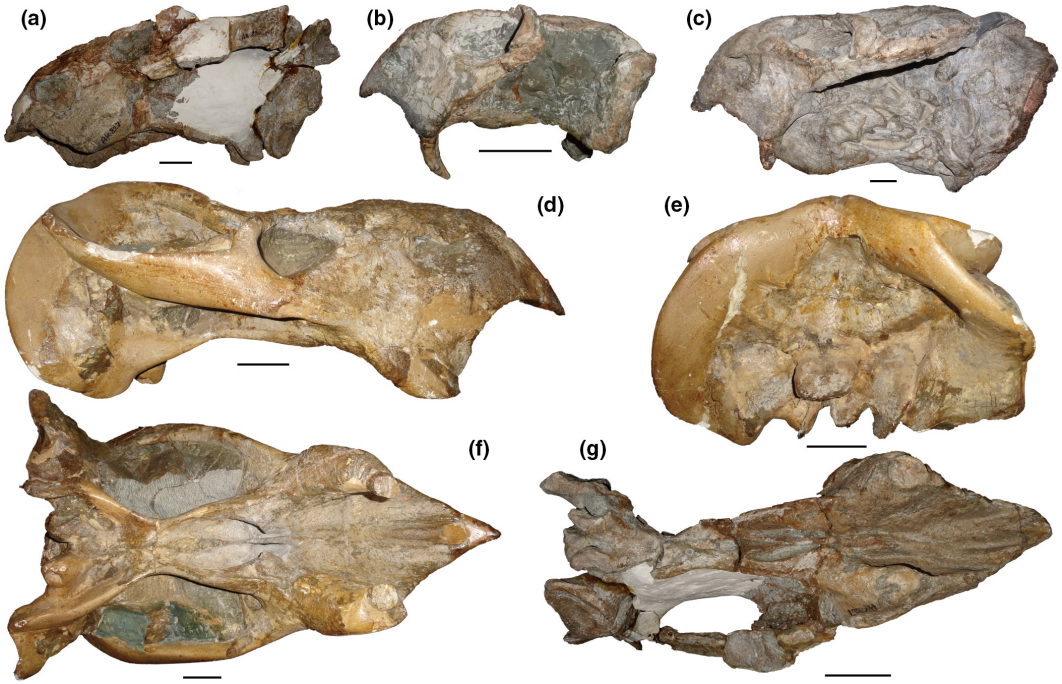

Fig 5. Photos of *Dinanomodon gilli* in lateral (a–d), posterior (e) and ventral views (f, g): (a, g) CGS AK82-7; (b) RC 22; (c) SAM-PK-K10220; (d–f) RC 9. Scale bars equal 5 cm.

contacts the footplate posteriorly. A similar epipterygoid is present in *Turfanodon*, *Daptocephalus*, *Idelesaurus* and *Odontocyclops*. However, in all these taxa except *Turfanodon*, the quadrate ramus lacks this sheet-like structure (Ewer, 1961; Angielczyk, 2002; Liu, 2021; personal observation). The epipterygoids in *Rhachiocephalus* and *Kitchinganomodon* lack the dorsal processes of the footplates (Maisch, 2002, 2005).

In occipital view, the cranial width is significantly greater than the height, resulting in a typical 'low-cranial' shape (Fig. 2c,d). The dorsal margin of the occiput forms an eave-like structure composed of the tabulars, squamosals and postparietal. The postparietal projects beyond the eave-like structure and reaches the largest width on the occipital plate. *Pelanomodon* and *Odontocyclops* have similar postparietals, which are partially surrounded by supraoccipitals (Angielczyk, 2002; Kammerer et al., 2015). However, their postparietals do not reach a similar relative width on the occipital plate as in *Dinanomodon*. The occipital plate portion of the postparietal is depressed. Similar depressions are also observed in *Din. gilli* (Fig. 5). The tabular is confined to the dorsal protruding portion, contacting the postparietal medially, the squamosal laterally and dorsally and the supraoccipital ventrally. The supraoccipital is a single large element, which features a concave postparietal-supraoccipital suture and forms the dorsal margin of the foramen magnum. The prootic and opisthotic are fused into the periotic, as in many other dicynodonts. In lateral view, the periotic is separated from the parietal by the supraoccipital (Fig. 2a,b). Its anterior edge is broken, leaving the pila antotica partially preserved. In posterior view, the periotics are positioned lateral to the exoccipitals, forming a pair of wing-like elements that contribute to the post-temporal fenestrae alongside the squamosals (Fig. 2c,d). The paroccipital process is complete on the left side, lying ventral to the post-temporal fenestra. It projects posteriorly out of the occiput, forming a bulge on its margin, as in other dicynodonts. The exoccipital contributes to the ventral portion of the foramen magnum and entirely encloses the jugular foramen, similar to *Euptychognathus kingae* ('*Dicynodon trigonocephalus*' of King (1981)), *Jimusaria* and *Oudenodon* (Keyser, 1975; Shi and Liu, 2023; Kammerer et al., 2025), but differs from *Lystrosaurus* and most basal dicynodonts. In many dicynodonts, the exoccipital forms the wall of the jugular foramen together with the periotic or opisthotic (Cluver, 1971; Angielczyk and Kammerer, 2017; Angielczyk et al., 2021a; Macungo et al., 2022); in some cases, the basioccipital also contributes to it, as seen in *Eosimops*, *Diictodon* (contra Sullivan and Reisz (2005)), *Pristerodon*, *Myosaurus*, *Cistecephalus* (but see Broili and Schröder (1935a)) and *Kawingasaurus* (Brink, 1950; Angielczyk and Rubidge, 2013; Macungo et al., 2022; Macungo et al., 2023). The jugular foramen perforates the dorsolateral base of the occipital condyle. The occipital

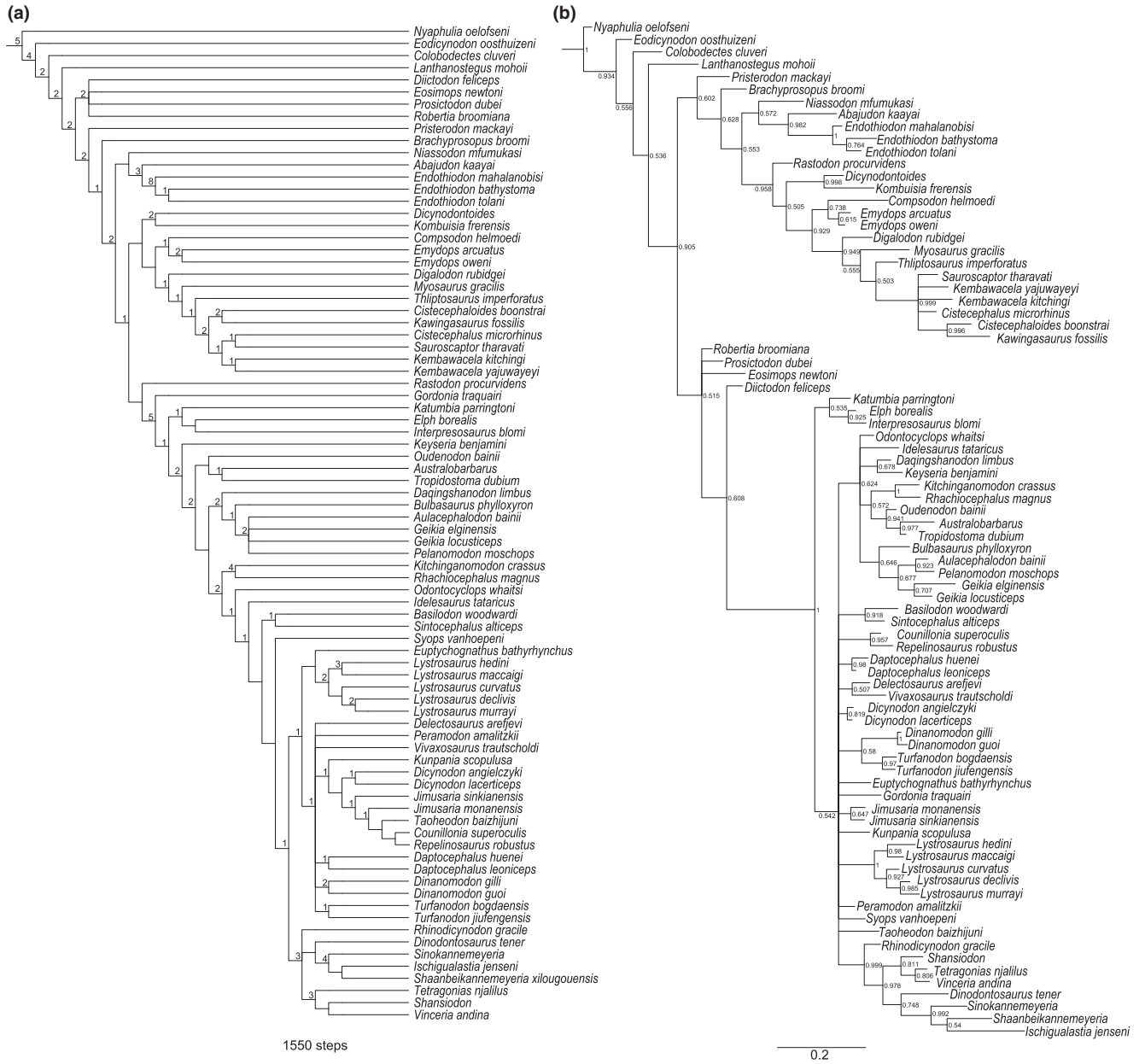

Fig 6. Phylogenetic trees of dicynodonts. (a) Strict consensus parsimonious tree. The node numbers represent Bremer support values greater than 0; (b) non-calibrated Bayesian phylogenetic tree. The node numbers represent posterior probability; the scale bar is in units of substitutions per character.

condyle is formed by the exoccipital and the basioccipital, but only a vague tripartite shape can be discerned; no distinct sutures are evident.

Phylogenetic analysis

The new matrix produced comparable results across different methods (Figs 6 and 7) and recovered most of the major groups identified in previous studies that used the matrix from Kammerer et al. (2011). *Nyaphulia* was recovered as the most basal dicynodont. *Din. guoi* formed the sister group of *Din. gilli* (Figs 6 and 7). The taxon definitions follow Kammerer and Angielczyk (2009).

Parsimony method—A total of 432 most parsimonious trees (MPTs), each with 1510 steps, were produced. The strict consensus tree (Fig. 6a) has 1550 steps.

Pylaecephalidae was recovered as a monophyletic group, but pylaecephalids form a polytomy. The

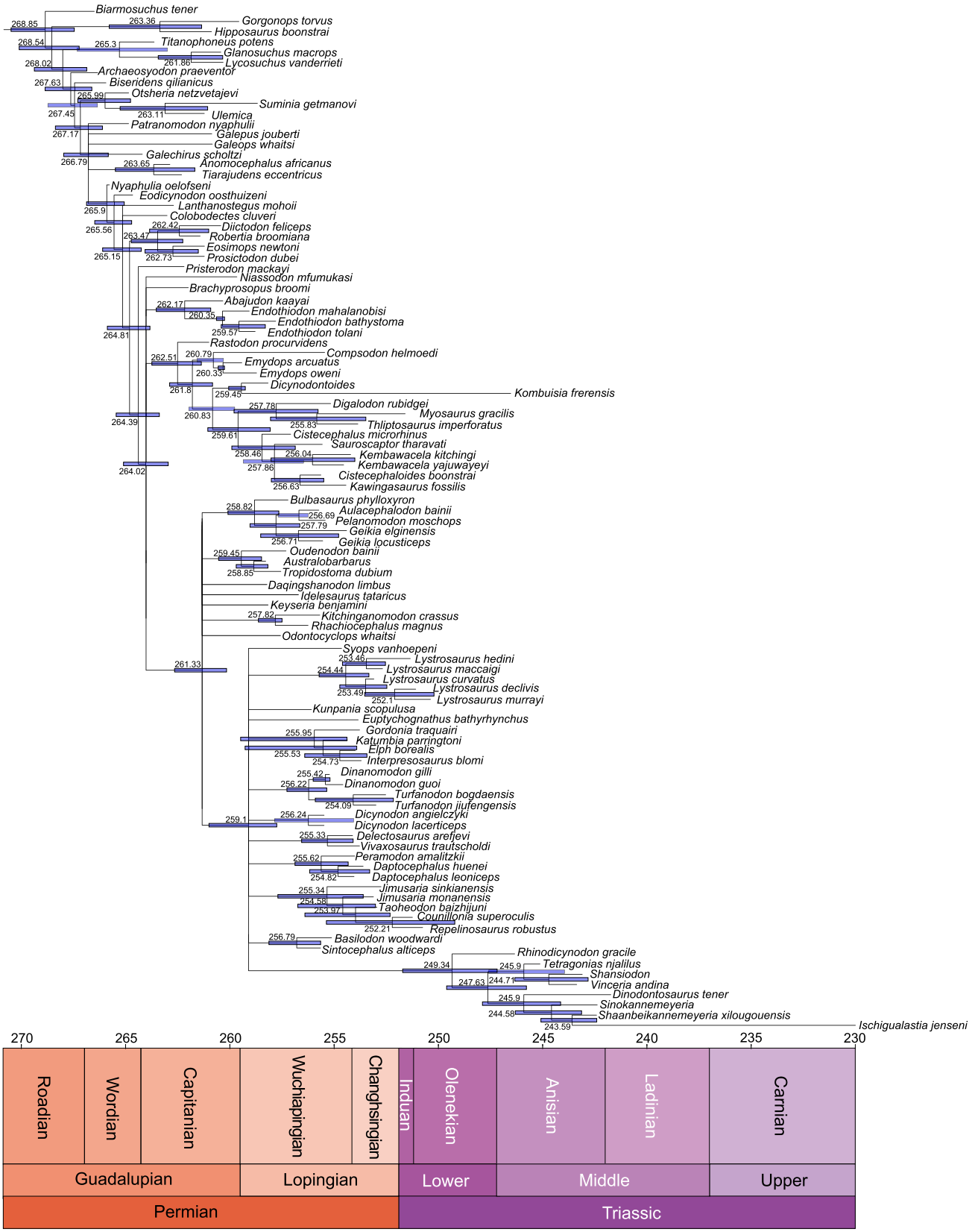

Fig 7. Calibrated phylogenetic tree of anomodonts. The node numbers represent the divergence time of these clades; the blue bars represent the 95% highest posterior density intervals (HPD); all ages are given in Ma.

Table 2
The 95% HPD, mean and median divergence time from tip-dating analysis of major clades

Node	Lower (Ma)	Upper (Ma)	Mean (Ma)	Median (Ma)
Anomodontia	266.62	268.86	267.68	267.63
Dicynodontia	265.07	266.87	265.92	265.90
Pylaecephalidae	262.45	264.65	263.50	263.47
Endothiodontia	260.92	263.53	262.20	262.17
Emydopoidea	261.37	263.74	262.54	262.51
Cistecephalidae	256.86	259.91	258.46	258.46
Bidentalia	260.16	262.65	261.37	261.33
Dicynodontiodea	257.75	261.00	259.22	259.10
Dinanomodon + *Turfanodon*	255.35	257.26	256.29	256.22
Dinanomodon	253.70	256.25	255.25	255.43
Lystrosaurus	253.33	255.72	254.48	254.44
Kannemeyeriiformes	247.19	251.71	249.41	249.34

topology of Endothiodontia is identical to that recovered by Maharaj et al. (2024). Emydopoidea was recovered as the sister group of Bidentalia. *Digalodon*, *Myosaurus* and *Thliptosaurus* were recovered basal to Cistecephalidae.

Contrary to recent results (Macungo et al., 2022), *Rastodon* was recovered as the most basal bidentalian again, but with a low support value. The supported synapomorphies are Ch. 205 (1 → 2) and 209 (2 → 4) (Fig. S1). Excluding *Rastodon*, the other bidentalians are supported by the synapomorphies Ch. 17 (1 → 0), 31 (1 → 0), 33 (0 → 1), 71 (0 → 1), 72 (0 → 1), 73 (0 → 1), 106 (1 → 0), 119 (4 → 2), 126 (1 → 2), 127 (0 → 1) (Fig. S1). *Gordonia* was also nested in a relatively basal position. The 'elphids' (*Katumbia*, *Interpresosaurus* and *Elph*) form a monophyletic group that is supported by the synapomorphies Ch. 20 (0 → 1) and 129 (0 → 1) (Fig. S1). They were recovered in a more derived position than *Gordonia*, but a more basal position than the other bidentalians. A paraphyletic Cryptodontia was recovered. Lystrosauridae form the sister group of the 'core-*Dicynodon*' clade. *Kunpania* was also positioned in that clade, rather than among the most basal bidentalians or dicynodontoids. *Jimusaria* was assembled with *Taoheodon* and the Laotian dicynodontoids (*Counillonia* and *Repelinosaurus*) as a basal grade. *Daptocephalus*, *Dinanomodon*, *Turfanodon* and some Russian dicynodontoids formed a polytomy in the 'core-*Dicynodon*' clade. The *Dinanomodon* clade is supported by Ch. 12 (0,1 → 2), 76 (1 → 2), 90 (0 → 1) (Fig. S1).

Kannemeyeriiformes became the sister group of the 'core-*Dicynodon*' clade + Lystrosauridae. Within Kannemeyeriiformes, a monophyletic Shansiodontidae (sensu Cox and Parrington (1965)) was recovered.

Bayesian inference—The majority rule consensus tree (Fig. 6b) shows a less resolved topology. Endothiodontia, Emydopoidea, *Brachyprosopus* and *Pristerodon* formed a monophyletic group. The topologies of Endothiodontia and Emydopoidea were basically consistent with those of the strict consensus parsimony tree. *Rastodon* was recovered as the most basal emydopoid. Pylaecephalids form a paraphyletic group outside Bidentalia; *Diictodon* was recovered as the sister group of Bidentalia. A monophyletic Cryptodontia was recovered. Geikiidae, Oudenodontidae plus Rhachiocephalidae and *Daqingshanodon* plus *Keyseria* were recovered as monophyletic groups, respectively, but formed a polytomy together.

Dicynodontoidea was recovered but displayed a large polytomy. *Dinanomodon* was recovered as the sister group of *Turfanodon*. A monophyletic *Jimusaria* was recovered again. *Gordonia* was placed in a polytomy within the Bidentalia clade. The *Lystrosaurus* clade shows the same topology as the parsimony result. The 'core-shansiodontid' (*Shansiodon*, *Vinceria* and *Tetragonias*) topology is similar to that of the MPTs, although *Rhinodicynodon* was recovered as the most basal kannemeyeriiform.

Bayesian tip-dating—The topology is basically the same as that of the non-calibrated analysis (Fig. 7). Pylaecephalidae was recovered as a monophyletic group. The sister group of Bidentalia remains unresolved. *Jimusaria* became a paraphyletic group and was positioned basal to *Taoheodon* plus the Laotian dicynodonts, as in the MPTs.

The origin of anomodonts was estimated at approximately 267.45 Ma, correlating with the Roadian. The most basal dicynodont, *Nyaphulia*, split from other dicynodonts at approximately 265.9 Ma. The origin ages of pylaecephalids, endothiodonts, emydopoids (including *Rastodon*) and cistecephalids were estimated at approximately 263.47, 262.17, 262.51 and 258.46 Ma, respectively (Fig. 7, Table 2). The time of origin for bidentalians was estimated at approximately 261.34 Ma (Capitanian), which is much younger than previous estimates (Boos et al., 2016; Griffin and Angielczyk, 2019; Angielczyk et al., 2021b). The divergence of cryptodonts and dicynodontoids occurred nearly simultaneously, at approximately 260–259 Ma,

correlating with the late Capitanian to early Wuchiapingian.

Dinanomodon and *Turfanodon* diverged at approximately 256.2 Ma. The divergence between *Din. gilli* and *Din. guoi* occurred around 255.41 Ma. Detailed information is provided in Table 2.

Discussion

The validation of Dinanomodon guoi

Dinanomodon has thus far only been reported from the Karoo Basin of South Africa (Kammerer et al., 2011). IVPP V31930 was discovered in North China, which was ~20 000 km away from the Karoo Basin during the Changhsingian (Scotese et al., 2024). IVPP V31930 is referred to *Dinanomodon* based on the low cranium with a frontal-premaxilla contact, a pointed and strongly hook-like snout tip and a postparietal partly surrounded by the supraoccipital. However, IVPP V31930 also shows several differences from *Din. gilli*: absence of caniniform buttress; lateral margin of subtemporal bar ventrally deflected; small postparietal contribution to intertemporal bar; and lacrimal boss confluent with prefrontal boss. The phylogenetic analysis in both parsimony and Bayesian methods supports IVPP V31930 as the sister species of *Din. gilli*.

Paleoecological and biostratigraphic implications

One of the most notable characters of *Dinanomodon* is the sharp, hook-like anterior tip of the snout (Fig. 1c). This character was previously known only in the Triassic kannemeyeriiform *Placerias* (Camp and Welles, 1956). Although the Permian *Keyseria* has a triangular premaxilla, it is not as pointed as that of *Dinanomodon* (Kammerer et al., 2011). Kemp (2005) proposed that such a pointed snout might indicate *Dinanomodon* as a browser, suggesting a preference for higher-growing foliage. Compared with other browsers like *Oudenodon* (Hotton, 1986; DeFauw, 1989), this unique snout tip may reflect a specialized diet and niche partitioning. Analogous beaks in ceratopsian dinosaurs have been interpreted as adaptations for browsing (Mallon and Anderson, 2014b; Cullen et al., 2022) and associated with high-fibre foliage consumption based on the dental morphology (Mallon and Anderson, 2014a). However, most of them also possess pointed predentaries that form sharp mandibular tips (Nabavizadeh, 2023). Parrots (Psittaciformes) exhibit beaks that are strikingly similar to those of *Dinanomodon*, especially the calyptorhynchid bill type characterized by a strongly curved, short and narrow upper bill and a dipper-shaped lower bill (Homberger, 2003). The narrow tip of this upper bill can penetrate and rip the thick wall of fruits to access seeds (Homberger, 2003). Based on this strong similarity, we deduce that *Dinanomodon* may have preferred seeds encased in high-fibrous walls. Some smaller specimens of *Dinanomodon* have blunt, rounded snouts (Kammerer et al., 2011), possibly indicating an ontogenetic dietary shift from generalists to specialists with growth. This hypothesis remains tentative due to limited evidence.

Dinanomodon represents the third reported Permian dicynodont genus (after *Diictodon* and *Geika*) shared between the Northern and Southern Hemispheres. The Chinese specimen suggests the extraordinary dispersal capability and adaptability of *Dinanomodon*, which could disperse over 20 000 km and crossed at least three climatic zones (Fig. 8) (Roscher et al., 2011; Huang et al., 2018; Liu et al., 2021; Scotese et al., 2024). These reported Chinese dicynodonts (Liu, 2021; Shi and Liu, 2023) challenge the hypothesis that dicynodonts preferred high latitudes (Bernardi et al., 2017), highlighting sampling bias in intermediate paleolatitudes.

Two tetrapod species, *Moschowhaitsia lidaqingi* (Liu and Abdala, 2023) and *Din. guoi* have been reported from the putative Sunan Formation of central Gansu Province. The coexistence of an apex predator and a large herbivore implies high ecosystem productivity of this region. However, the strata at their type locality differ significantly from the Sunan Formation's holostratotype (Sunan County, Gansu Province) (Bureau of Geology and Mineral Resources of Gansu Province, 1989; Liu et al., 2012), highlighting the need for formal stratigraphic reassessment.

The *Dinanomodon* occurrence constrains this fossil bed to the Lopingian, correlating with the upper *Cistecephalus* AZ to the *Daptocephalus* AZ in South Africa (Smith, 2020; Viglietti, 2020). Furthermore, the time interval of the fossil bed is further constrained between 255.2 and 252.24 Ma (Rubidge et al., 2013; Gastaldo et al., 2020).

Phylogeny of bidentalians

Bidentalia is a well-supported clade (Figs 6 and 7), but Bayesian inference reveals uncertainty regarding its sister group.

Boos et al. (2016) proposed *Rastodon* as the most basal bidentalian, a placement supported by subsequent phylogenies (Angielczyk and Kammerer, 2017; Kammerer et al., 2019; Kammerer, 2019a; Kammerer, 2019b; Kammerer and Ordoñez, 2021; Liu, 2021; Angielczyk et al., 2021b; Shi and Liu, 2023; Szczygielski and Sulej, 2023). However, this position is disputed (Kammerer and Ordoñez, 2021) and some recent analyses suggest alternative positions, such as in

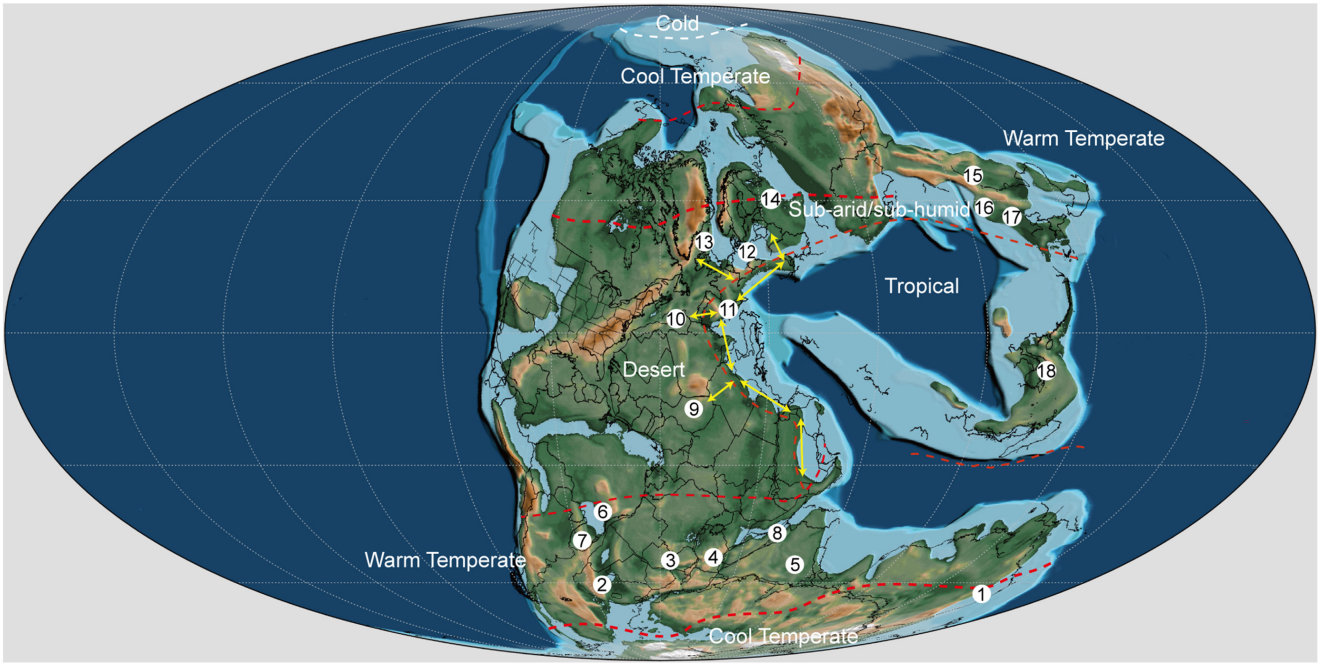

Fig 8. Paleogeographic reconstruction of Wuchiapingian from Scotese et al. (2024) with major Lopingian tetrapod localities and climatic zones (modified from Roscher et al. (2011), Bernardi et al. (2017), Liu et al. (2021), Scotese et al. (2024)). Localities: 1, Sydney Basin, Australia; 2, Karoo Basin, South Africa; 3, Zambia and Zimbabwe; 4, Malawi and Tanzania; 5, Pranhita-Godavari and Satpura basins, India; 6, Paraná Basin, Brazil; 7, Uruguay; 8, Madagascar; 9, Tim Mersoi Basin, Niger; 10, Argana Basin, Morocco; 11, Italy; 12, Germany and Poland; 13, Scotland; 14, Cis-Urals Basin, Russia; 15, Junggar Basin, China; 16, Alxa Block, China; 17, Ordos Basin, China; 18, Laos. Yellow arrows indicate the cross-equatorial routes.

Emydopoidea (Macungo et al., 2022) or as the sister group of Therochelonia (Macungo et al., 2023). Our parsimony analysis recovered the original hypothesis (Fig. 6a). Two discretized continuous characters, the relative length of the interpterygoid vacuity and the ratio of maximum height of the postdentary bones to the dentary ramus, support this topology (Fig. S1). These two continuous characters also supported bidentalian affinity in previous phylogenies. In our analysis, bidentalians indeed share the same character states with *Rastodon* after discretizing these two characters; however, Bayesian inferences still support emydopoid affinity (Figs 6b and 7; posterior probability = 0.944/0.812). These conflicting topologies indicate the lack of informative characters for phylogeny in this part of the tree.

The variable placement of *Kunpania*, from the most basal bidentalian (Angielczyk et al., 2021b), to the most basal dicynodontoid (Shi and Liu, 2023), to a derived dicynodontoid (in our analyses; Figs 6 and 7), should be attributed to its being only known from a fragmentary skull.

The monophyly of Cryptodontia and the systematic position of the 'elphids' are two persistent issues in bidentalian phylogeny (Angielczyk and Kammerer, 2017). Our analyses failed to recover Cryptodontia as a monophyletic group except in non-calibrated Bayesian inference (Figs 6 and 7), though the major cryptodont families were consistently recovered. Enigmatic 'Elphidae' exhibits notable topological instability across analyses (Figs 6 and 7), while tip-dating methods grouped *Gordonia* with these taxa (Fig. 7). The variable positions identified under parsimony and Bayesian frameworks suggest that the current dataset lacks sufficient informative characters to resolve the positions of these taxa. This systematic ambiguity underscores the need for comprehensive taxonomic revisions focusing on cryptodonts.

Dicynodontoid phylogeny remains contentious despite the milestone revision by Kammerer et al. (2011). Persistent ambiguities affect interpretations regarding the relationships of non-African taxa, the systematic position of *Dicynodon*, the origin of *Lystrosaurus* and kannemeyeriiforms, etc. Contrary to the results of George et al. (2025), *Gordonia* does not nest within *Jimusaria*, though it obtains several variable positions (Figs 6 and 7). We also note that *Gordonia* has an anterior process on the splenial symphysis, a pair of narrow dentary tables and a reduced median dentary groove (George et al., 2025), which is different from *Jimusaria* (Shi and Liu, 2023). The *Dinanomodon* plus *Turfanodon* clade is supported by Bayesian inferences (Figs 6b and 7), but shows instability under parsimony (Fig. 6a). The synapomorphies of the

Turfanodon plus *Dinanomodon* clade in those MPTs that include it are: notch on dorsal edge of narial opening present; contact of premaxilla and frontals; contact of postorbital and squamosal in the base of the postorbital bar; similar height of anterior pterygoid keel in lateral view relative to the height of the non-keel ramus. One of the most notable synapomorphies of the *Dinanomodon* plus *Turfanodon* clade is the contact between the premaxilla and frontals, but this character also appears in some taxa as individual variation (see Broili and Schröder (1935b) for *Pristerodon*), so the monophyly of this clade still needs careful investigation, though it is stable in previous analyses (Liu, 2020; Kammerer and Ordoñez, 2021; Liu, 2021; Angielczyk et al., 2021b; Liu, 2022; Macungo et al., 2022; Escobar et al., 2023; Shi and Liu, 2023; Szczygielski and Sulej, 2023; George et al., 2025). *Jimusaria* is posited in a new position as a paraphyletic group in two of our topologies, though this topology receives weak support (Fig. 6a). These inconsistencies highlight the need for expanded character data.

The monophyly of Shansiodontidae is one of several unresolved questions for kannemeyeriiforms. Our results exclude *Rhinodicynodon* from this family (Figs 6 and 7). *Rhinodicynodon* is a poorly studied taxon, and further comparative research on all shansiodontid materials will be beneficial for resolving its taxonomy and relationships.

The divergence and dispersal of bidentalians

Our novel tip-dating analysis estimates anomodont origins at approximately 267.45 Ma (Roadian) (Fig. 7), younger than the result obtained by Matamales-Andreu et al. (2024). Notably, bidentalians originated ~261.34 Ma (Capitanian), ~1.2 Myr prior to the initial eruption of the Emeishan large igneous province (ELIP) (Huang et al., 2022). The ELIP is linked to the end-Guadalupian extinction (Wignall et al., 2009; Ling et al., 2023; Li et al., 2024). In terrestrial ecosystems, this crisis is characterized by dinocephalian extinction globally (Lucas, 2009), and in the Karoo Basin, this crisis occurred ~260.26 Ma (Day et al., 2015). Dicynodontoids and major cryptodont clades originated after ~260 Ma (Fig. 7), suggesting that the vacant niches incurred by this crisis might have driven their radiation.

The earliest cryptodonts are represented by *Australobarbarus* (Fig. 7) from the Kotelnich Fauna of the Cis-Urals Basin, which belongs to Laurasia. This might be the earliest record of bidentalians as well (Davydov et al., 2020), depending on the ages and phylogenetic positions of *Rastodon* and *Kunpania*. The closest relatives of *Australobarbarus* (*Oudenodon* and *Tropidostoma*) are from Gondwana. Considering the close relationship between these three taxa (Botha and Angielczyk, 2007), this clade could be considered the earliest record of cross-equatorial dispersal of bidentalians at low taxonomic levels, occurring at ~258 Ma (constrained by the age of the *Tropidostoma* – *Gorgonops* Subzone (Day et al., 2015)). Subsequent *Geikia* dispersal postdated ~256.71 Ma. Within Dicynodontoidea, due to the lack of bifurcated topology, we cannot detect the divergence times of higher taxonomic clades. The dispersal of *Dinanomodon* postdated ~255.41 Ma; if the *Dinanomodon* plus *Turfanodon* clade originated in Laurasia, then this dispersal would be constrained to 255.41–255.2 Ma (the age from the lower *Dicynodon* – *Theriognathus* Subzone (Rubidge et al., 2013)).

The *Lystrosaurus* clade originated at ~254.42 Ma (Wuchiapingian). Despite its occurrence in the Karoo Basin during the late Permian, all well-constrained Laurasian records are Early Triassic in age (Angielczyk et al., 2022; Shishkin et al., 2024), leaving its dispersal timing unresolved.

Diictodon represents the only basal dicynodont genus with cross-equatorial dispersal, documented outside Gondwana only in the Junggar Basin of China (Angielczyk and Sullivan, 2008). This taxon exhibits an extensive stratigraphic range in the Karoo Basin (from the *Tapinocephalus* AZ to the *Daptocephalus* AZ (Smith et al., 2020)), while the stratigraphic position of the Chinese specimen remains uncertain and can only be assigned to the upper Permian (Li et al., 2008).

Cross-equatorial tetrapod dispersal during the Lopingian

Pangaea enabled potentially global terrestrial tetrapod distributions. Several cases of shared tetrapod sister-taxa between Laurasia and Gondwana are currently recognized, but few at the genus level (Liu and Abdala, 2022). Beyond the dicynodonts mentioned above, recent reports of the large gorgonopsian *Inostrancevia* from the Karoo Basin provided the first evidence of this genus outside of Russia (Kammerer et al., 2023). The South African specimens are restricted to the *Daptocephalus* AZ, but additional, subsequently described specimens from Tanzania and Mozambique indicate potentially earlier appearances and wider distribution (Brant and Sidor, 2023; Macungo et al., 2025).

The akidnognathid therocephalian *Euchambersia* is another example of cross-equatorial distribution, with occurrences in both South Africa (*Cistecephalus* AZ) and North China (Member I of the Naobaogou Formation), correlating with the Wuchiapingian age (Smith, 2020; Liu and Abdala, 2022).

Procynosuchus is a cosmopolitan cynodont, which is known from several localities in Gondwana (South Africa, Tanzania, Zambia) and Laurasia (Germany and Russia) (Abdala, 2021). *Procynosuchus* is an index fossil for the *Dicynodon–Theriognathus* Subzone of the Karoo Basin, and it appears in the Sokolki assemblage

of the Cis-Urals Basin. The radioisotopic ages of these two localities suggest that the cross-equatorial dispersal happened in the Wuchiapingian (Davydov et al., 2020; Gastaldo et al., 2020).

The expansive desert and extremely high temperature in the interior of Pangaea (Roscher et al., 2011; Bernardi et al., 2017) are thought to represent the major barriers to tetrapod dispersal at this time (Fig. 8). However, a narrow corridor with tropical seasonal or ever-wet climate could have existed along the eastern coast, based on climate zone reconstruction (Roscher et al., 2011; Bernardi et al., 2017; Liu et al., 2021; Scotese et al., 2024) and floral distribution (Rees et al., 2002; Bernardi et al., 2017). The central desert also had some oases at that time, such as the Tim Mersoi Basin in Niger (Tabor et al., 2011; Tsuji et al., 2013; Smith et al., 2015) and the Argana Basin in Morocco (Hmich et al., 2006; Voigt et al., 2010), which are rich in tetrapod records (including large amphibians indicative of standing water bodies). Those regions might have provided water and food supplies for some tolerant migrants, similar to modern desert elephants (*Loxodonta africana*) in the Namib and Sahara deserts (Benitez et al., 2022). Those tetrapod records shared between Laurasia and Gondwana indicate frequent exchange among faunas during the Lopingian.

Temperature fluctuations significantly influenced tetrapod diversity during the Permian–Triassic turnover (Benton and Newell, 2014; Liu et al., 2022; Simões et al., 2022). Some authors have also suggested that the Lopingian cooling may have affected tetrapod diversity (Viglietti et al., 2021; Liu et al., 2022). Cooling in low-latitude regions might facilitate the dispersal across arid zones, but the oxygen isotopic compositions exhibit spatially and temporally inconsistent responses to this cooling event (Chen et al., 2013; Chen et al., 2016; Wang et al., 2020). Some results constrain the cooling signal to the early Wuchiapingian (Viaretti et al., 2025), while others report no detectable cooling in equatorial areas (Joachimski et al., 2019; Chen et al., 2020). Furthermore, numerical simulations suggest that Lopingian temperature changes minimally affected tropical belts (Roscher et al., 2011), implying that a stable ecological corridor on the equator was unlikely to have collapsed due to this cooling.

Another key ecological factor is precipitation. The aridification trend in the Permian was interrupted by the Wuchiapingian wet phase (Hmich et al., 2006; Roscher and Schneider, 2006; Schneider et al., 2006). Around the equator, this wet phase facilitated the flourish of flora and provided habitats for tetrapods (Hmich et al., 2006; Bernardi et al., 2017). Thus, precipitation, rather than temperature, appears to have been the major climate factor controlling dispersal between the Northern and Southern Hemispheres during the Guadalupian and Lopingian. This scenario can also explain why the shared Guadalupian tetrapod genus records between the Northern and Southern Hemispheres are rare (Olroyd and Sidor, 2017): persistent aridification in low-latitude regions resulted in the collapse of low-latitude florae and the formation of a vast arid zone (Scotese et al., 2024). It also correlates with Brocklehurst et al. (2018), who noted that the tetrapod vicariance rate peaked during the Capitanian and then dramatically dropped during the Wuchiapingian. They also suggested this variation was influenced by the climate.

Conclusion

A new dicynodont species, *Dinanomodon guoi*, is established based on a specimen collected in Gulang County, Gansu Province, China. This discovery marks the first bidentalian genus shared between China and South Africa.

The phylogeny of bidentalians is unresolved, with the lack of informative characters in this part of the tree being the major issue. We will continue revising non-kannemeyeriiform dicynodont datasets to resolve these complex relationships.

Tip-dating analysis suggests that diversification of the bidentalians took place after the end-Guadalupian extinction, but their origin occurred prior to the ELIP.

The cross-equatorial dispersal of Lopingian tetrapods was more frequent than previously thought, and the ecological corridor along the eastern margin of Pangaea had capacity for carrying the large animals' dispersal (e.g. *Dinanomodon*, *Inostrancevia*). We emphasize the importance of precipitation, rather than temperature, as the major controlling factor of the cross-equatorial dispersal of tetrapods during the Permian.

Acknowledgements

We gratefully thank the members of the field team to Jingtai in 2020, Fu Hua-Lin for preparation and Gao Wei for photography. We also sincerely thank Zhang Chi for helpful assistance in Bayesian inference and Christian Kammerer for generously sharing photos of *Dinanomodon gilli*. The comments and edits from an anonymous reviewer and Christian Kammerer improved the manuscript. This work was supported by the International Partnership Program of the Chinese Academy of Sciences (132311KYSB20190010).

Conflict of interest

The authors declare that they have no conflict of interest.

Data availability statement

The data that supports the findings of this study are available in Supporting Information of this article.

References

Abdala, F., 2021. Permo-Jurassic cynodonts: the early road to mammalness. In: Alderton, D. and Elias, S.A. (Eds.), Encyclopedia of Geology, second edition. Academic Press, London, UK. pp. 206–226.

Angielczyk, K.D., 2002. Redescription, phylogenetic position, and stratigraphic significance of the dicynodont genus *Odontocyclops* (Synapsida: Anomodontia). J. Paleontol. 76, 1047–1059.

Angielczyk, K.D. and Kammerer, C.F., 2017. The cranial morphology, phylogenetic position and biogeography of the upper Permian dicynodont *Compsodon helmoedi* van Hoepen (Therapsida, Anomodontia). Pap. Palaeontol. 3, 513–545.

Angielczyk, K.D. and Kurkin, A.A., 2003. Phylogenetic analysis of Russian Permian dicynodonts (Therapsida: Anomodontia): implications for Permian biostratigraphy and Pangaean biogeography. Zool. J. Linnean Soc. 139, 157–212.

Angielczyk, K.D. and Rubidge, B.S., 2013. Skeletal morphology, phylogenetic relationships and stratigraphic range of *Eosimops newtoni* Broom, 1921, a pylaecephalid dicynodont (Therapsida, Anomodontia) from the Middle Permian of South Africa. J. Syst. Palaeontol. 11, 191–231.

Angielczyk, K.D. and Sullivan, C., 2008. *Diictodon feliceps* (Owen, 1876), a dicynodont (Therapsida, Anomodontia) species with a Pangaean distribution. J. Vertebr. Paleontol. 28, 788–802.

Angielczyk, K.D., Benoit, J., Rubidge, B.S. and Ruta, M., 2021a. A new tusked cistecephalid dicynodont (Therapsida, Anomodontia) from the upper Permian upper Madumabisa Mudstone formation, Luangwa Basin, Zambia. Pap. Palaeontol. 7, 405–446.

Angielczyk, K.D., Liu, J. and Yang, W., 2021b. A redescription of *Kunpania scopulusa*, a bidentalian dicynodont (Therapsida, Anomodontia) from the ?Guadalupian of northwestern China. J. Vertebr. Paleontol. 41, e1922428.

Angielczyk, K.D., Liu, J., Sidor, C.A. and Yang, W., 2022. The stratigraphic and geographic occurrences of Permo-Triassic tetrapods in the Bogda Mountains, NW China – Implications of a new cyclostratigraphic framework and Bayesian age model. J. Afr. Earth Sci. 195, 104655.

Angielczyk, K.D., Peecook, B.R. and Smith, R.M.H., 2023. The mandible of *Compsodon helmoedi* (Therapsida: Anomodontia), with new records from the Ruhuhu Basin, Tanzania. Palaeontol. Afr. 56, 88–102.

Archie, J.W., 1985. Methods for coding variable morphological features for numerical taxonomic analysis. Syst. Zool. 34, 326–345.

Bardin, J., Rouget, I., Yacobucci, M.M. and Cecca, F., 2014. Increasing the number of discrete character states for continuous characters generates well-resolved trees that do not reflect phylogeny. Integr. Zool. 9, 531–541.

Benitez, L., Kilian, J.W., Wittemyer, G., Hughey, L.F., Fleming, C.H., Leimgruber, P., du Preez, P. and Stabach, J.A., 2022. Precipitation, vegetation productivity, and human impacts control home range size of elephants in dryland systems in northern Namibia. Ecol. Evol. 12, e9288.

Benton, M.J. and Newell, A.J., 2014. Impacts of global warming on Permo-Triassic terrestrial ecosystems. Gondwana Res. 25, 1308–1337.

Bernardi, M., Petti, F.M., Kustatscher, E., Franz, M., Hartkopf-Fröder, C., Labandeira, C.C., Wappler, T., van Konijnenburg-van Cittert, J.H., Peecook, B.R. and Angielczyk, K.D., 2017. Late Permian (Lopingian) terrestrial ecosystems: a global comparison with new data from the low-latitude Bletterbach Biota. Earth Sci. Rev. 175, 18–43.

Boos, A.D., Kammerer, C.F., Schultz, C.L., Soares, M.B. and Ilha, A.L., 2016. A new dicynodont (Therapsida: Anomodontia) from the Permian of Southern Brazil and its implications for bidentalian origins. PLoS One 11, e0155000.

Botha, J. and Angielczyk, K.D., 2007. An integrative approach to distinguishing the dicynodont species *Oudenodon bainii* and *Tropidostoma microtrema* (Therapsida: Anomodontia). Palaeontology 50, 1175–1209.

Brant, A.J. and Sidor, C.A., 2023. Earliest evidence of *Inostrancevia* in the southern hemisphere: new data from the Usili Formation of Tanzania. J. Vertebr. Paleontol. 43, e2313622.

Brink, A.S., 1950. XCI.—on a new species of *Cistecephalus* Owen. Ann. Mag. Nat. Hist. 3, 985–997.

Brocklehurst, N., Dunne, E.M., Cashmore, D.D. and Frbisch, J., 2018. Physical and environmental drivers of Paleozoic tetrapod dispersal across Pangaea. Nat. Commun. 9, 5216.

Broili, F. and Schröder, J., 1935a. Beobachtungen an Wirbeltieren der Karrooformation. VI. Über den Schädel von *Cistecephalus* Owen. Sitzungsberichte der Bayerischen Akademie der Wissenschaften Mathematisch-Naturwissenschaftliche Abteilung, Germany.

Broili, F. and Schröder, J., 1935b. Beobachtungen an Wirbeltieren der Karrooformation. XII. Über Einige Primitive Anomodontier-Schädel aus den Unteren Beaufort-Schichten. Sitzungsberichte der Bayerischen Akademie der Wissenschaften Mathematisch-Naturwissenschaftliche Abteilung, Gemany.

Broom, R., 1932. The Mammal-Like Reptiles of South Africa and the Origin of Mammals. H. F. & G. Witherby, UK.

Broom, R., 1938. On two new anomodont genera. Ann. Transv. Mus. 19, 247–250.

Broom, R., 1940a. On some new genera and species of fossil reptiles from the Karroo beds of Graaff-Reinet. Ann. Transv. Mus. 20, 157–192.

Broom, R., 1940b. Some new Karroo reptiles from the Graaff-Reinet District. Ann. Transv. Mus. 20, 71–87.

Broom, R. and Robinson, J.T., 1948. Some new fossil reptiles from the Karoo beds of South Africa. Proc. Zool. Soc. London 118, 392–407.

Bureau of Geology and Mineral Resources of Gansu Province, 1989. Regional Geology of Gansu Province. Geological Publishing House, China.

Camp, C.L. and Welles, S.P., 1956. Triassic dicynodont reptiles. Part 1, the North American genus *Placerias*. Mem. Univ. Calif. 13, 255–304.

Chen, J. and Liu, J., 2024. Journey to the east: the oldest tetrapod fauna of east Pangea in early Permian. Natl. Sci. Rev. 11, nwae249.

Chen, B., Joachimski, M.M., Shen, S.-z., Lambert, L.L., Lai, X.-l., Wang, X.-d., Chen, J. and Yuan, D.-x., 2013. Permian ice volume and palaeoclimate history: oxygen isotope proxies revisited. Gondwana Res. 24, 77–89.

Chen, J., Shen, S.-z., Li, X.-h., Xu, Y.-g., Joachimski, M.M., Bowring, S.A., Erwin, D.H., Yuan, D.-x., Chen, B., Zhang, H., Wang, Y., Cao, C.-q., Zheng, Q.-f. and Mu, L., 2016. High-resolution SIMS oxygen isotope analysis on conodont apatite from South China and implications for the end-Permian mass extinction. Palaeogeogr. Palaeoclimatol. Palaeoecol. 448, 26–38.

Chen, J., Shen, S.-z., Zhang, Y.-c., Angiolini, L., Gorgij, M.N., Crippa, G., Wang, W., Zhang, H., Yuan, D.-x., Li, X.-h. and Xu, Y.-g., 2020. Abrupt warming in the latest Permian detected using high-resolution in situ oxygen isotopes of conodont apatite from Abadeh, central Iran. Palaeogeogr. Palaeoclimatol. Palaeoecol. 560, 109973.

Cluver, M.A., 1971. The cranial morphology of the dicynodont genus *Lystrosaurus*. Ann. S. Afr. Mus. 56, 155–274.

Cluver, M.A. and King, G.M., 1983. A reassessment of the relationships of Permian Dicynodontia (Reptilia, Therapsida) and a new classification of dicynodonts. Ann. S. Afr. Mus. 91, 195–273.

Colombi, C., Martínez, R.N., Césari, S.N., Alcober, O., Limarino, C.O. and Montañez, I., 2021. A high-precision U–Pb zircon age

constraints the timing of the faunistic and palynofloristic events of the Carnian Ischigualasto Formation, San Juan, Argentina. J. S. Am. Earth Sci. 111, 103433.
Cox, C.B. and Parrington, F.R., 1965. New Triassic dicynodonts from South America, their origins and relationships. Philos. Trans. R. Soc. Lond., Ser. B 248, 457–514.
Cullen, T.M., Zhang, S., Spencer, J., Cousens, B. and Button, D., 2022. Sr-O-C isotope signatures reveal herbivore niche-partitioning in a Cretaceous ecosystem. Palaeontology 65, e12591.
Davydov, V.I., Arefiev, M.P., Golubev, V.K., Karasev, E.V., Naumcheva, M.A., Schmitz, M.D., Silantiev, V.V. and Zharinova, V.V., 2020. Radioisotopic and biostratigraphic constraints on the classical middle–upper Permian succession and tetrapod fauna of the Moscow syneclise, Russia. Geology 48, 742–747.
Day, M.O. and Rubidge, B.S., 2020. Biostratigraphy of the *Tapinocephalus* Assemblage Zone (Beaufort Group, Karoo Supergroup), South Africa. S. Afr. J. Geol. 123, 149–164.
Day, M.O. and Smith, R.M.H., 2020. Biostratigraphy of the *Endothiodon* Assemblage Zone (Beaufort Group, Karoo Supergroup), South Africa. S. Afr. J. Geol. 123, 165–180.
Day, M.O., Ramezani, J., Bowring, S.A., Sadler, P.M., Erwin, D.H., Abdala, F. and Rubidge, B.S., 2015. When and how did the terrestrial mid-Permian mass extinction occur? Evidence from the tetrapod record of the Karoo Basin, South Africa. Proc. R. Soc. Lond. B Biol. Sci. 282, 20150834.
DeFauw, S.L., 1989. Patterns of evolution in the Dicynodontia, with special reference to austral taxa. Geol. Soc. Lond. Spec. Publ. 47, 63–84.
Duhamel, A., Benoit, J., Wynd, B., Wright, A.M. and Rubidge, B., 2024. Redescription of three basal anomodonts: a phylogenetic reassessment of the holotype of *Eodicynodon oelofseni* (NMQR 2913). Front. Earth Sci. 11, 1220341.
Escobar, J.A., Martinelli, A.G., Ezcurra, M.D., Fiorelli, L.E., Baczko, M.B.V., Novas, F.E. and Desojo, J.B., 2023. A reassessment of the mandibular anatomy of *Dinodontosaurus brevirostris* (Synapsida, Dicynodontia) from the Ladinian–early Carnian Chañares Formation (Northwestern Argentina), and its taxonomic and phylogenetic significance. Ameghiniana 60, 178–201.
Ewer, R.F., 1961. The anatomy of the anomodont *Daptocephalus leoniceps* (Owen). Proc. Zool. Soc. London 136, 375–402.
Felsenstein, J., 1988. Phylogenies and quantitative characters. Annu. Rev. Ecol. Evol. Syst. 19, 445–471.
Fröbisch, J., 2009. Composition and similarity of global anomodont-bearing tetrapod faunas. Earth Sci. Rev. 95, 119–157.
Gastaldo, R.A., Kamo, S.L., Neveling, J., Geissman, J.W., Looy, C.V. and Martini, A.M., 2020. The base of the *Lystrosaurus* Assemblage Zone, Karoo Basin, predates the end-Permian marine extinction. Nat. Commun. 11, 1428.
George, H., Kammerer, C.F., Foffa, D., Clark, N.D.L. and Brusatte, S.L., 2025. Micro-CT data reveal new information on the craniomandibular and neuroanatomy of the dicynodont *Gordonia* (Therapsida: Anomodontia) from the late Permian of Scotland. Zool. J. Linnean Soc. 203, zlae065.
Goloboff, P.A., 2024. Wincladtree: publication-quality tree-diagrams with TNT scripts. Cladistics 40, 438–442.
Goloboff, P.A. and Morales, M.E., 2023. TNT version 1.6, with a graphical interface for MacOS and Linux, including new routines in parallel. Cladistics 39, 144–153.
Goloboff, P.A., Mattoni, C.I. and Quinteros, A.S., 2006. Continuous characters analyzed as such. Cladistics 22, 589–601.
Griffin, C.T. and Angielczyk, K.D., 2019. The evolution of the dicynodont sacrum: constraint and innovation in the synapsid axial column. Paleobiology 45, 201–220.
Hendrixson, B.E. and Bond, J.E., 2009. Evaluating the efficacy of continuous quantitative characters for reconstructing the phylogeny of a morphologically homogeneous spider taxon (Araneae, Mygalomorphae, Antrodiaetidae, *Antrodiaetus*). Mol. Phylogenet. Evol. 53, 300–313.
Hmich, D., Schneider, J.W., Saber, H., Voigt, S. and El Wartiti, M., 2006. New continental Carboniferous and Permian faunas of Morocco: implications for biostratigraphy, palaeobiogeography and palaeoclimate. Geol. Soc. Lond. Spec. Publ. 265, 297–324.
Holvast, E.J., Celik, M.A., Phillips, M.J. and Wilson, L.A.B., 2024. Do morphometric data improve phylogenetic reconstruction? A systematic review and assessment. BMC Ecol. Evol. 24, 127.
Homberger, D.G., 2003. The comparative biomechanics of a prey-predator relationship: the adaptive morphologies of the feeding apparatus of Australian Black-Cockatoos and their foods as a basis for the reconstruction of the evolutionary history of the Psittaciformes. In: Bels, V.L., Gasc, J.-P. and Casinos, A. (Eds.), Vertebrate Biomechanics and Evolution. BIOS Scientific Publishers Ltd, Oxford, UK. pp. 203–228.
Hotton, N., III, 1986. Dicynodonts and their role as primary consumers. In: Hotton, N., III, MacLaren, P.D., Roth, J.J. and Roth, E.C. (Eds.), The Ecology and Biology of Mammal-Like Reptiles. Smithsonian Institute Press, Washington, DC, USA. pp. 71–82.
Huang, B., Yan, Y., Piper, J.D.A., Zhang, D., Yi, Z., Yu, S. and Zhou, T., 2018. Paleomagnetic constraints on the paleogeography of the East Asian blocks during Late Paleozoic and Early Mesozoic times. Earth Sci. Rev. 186, 8–36.
Huang, H., Huyskens, M.H., Yin, Q.-Z., Cawood, P.A., Hou, M., Yang, J., Xiong, F., Du, Y. and Yang, C., 2022. Eruptive tempo of Emeishan large igneous province, southwestern China and northern Vietnam: relations to biotic crises and paleoclimate changes around the Guadalupian-Lopingian boundary. Geology 50, 1083–1087.
Irmis, R.B., Mundil, R., Mancuso, A.C., Carrillo-Briceño, J.D., Ottone, E.G. and Marsicano, C.A., 2022. South American Triassic geochronology: constraints and uncertainties for the tempo of Gondwanan non-marine vertebrate evolution. J. S. Am. Earth Sci. 116, 103770.
Joachimski, M.M., Alekseev, A.S., Grigoryan, A. and Gatovsky, Y.A., 2019. Siberian Trap volcanism, global warming and the Permian-Triassic mass extinction: new insights from Armenian Permian-Triassic sections. Geol. Soc. Am. Bull. 132, 427–443.
Kammerer, C.F., 2019a. A new dicynodont (Anomodontia: Emydopoidea) from the terminal Permian of KwaZulu-Natal, South Africa. Palaeontol. Afr. 53, 179–191.
Kammerer, C.F., 2019b. Revision of the Tanzanian dicynodont *Dicynodon huenei* (Therapsida: Anomodontia) from the Permian Usili formation. PeerJ 7, e7420.
Kammerer, C.F. and Angielczyk, K.D., 2009. A proposed higher taxonomy of anomodont therapsids. Zootaxa 2018, 1–24.
Kammerer, C.F. and Ordoñez, M.d.l.A., 2021. Dicynodonts (Therapsida: Anomodontia) of South America. J. S. Am. Earth Sci. 108, 103171.
Kammerer, C.F. and Smith, R.M.H., 2017. An early geikiid dicynodont from the *Tropidostoma* Assemblage Zone (late Permian) of South Africa. PeerJ 5, e2913.
Kammerer, C.F., Angielczyk, K.D. and Fröbisch, J., 2011. A comprehensive taxonomic revision of *Dicynodon* (Therapsida, Anomodontia) and its implications for dicynodont phylogeny, biogeography, and biostratigraphy. J. Vertebr. Paleontol. 31, 1–158.
Kammerer, C.F., Angielczyk, K.D. and Fröbisch, J., 2015. Redescription of the geikiid *Pelanomodon* (Therapsida, Dicynodontia), with a reconsideration of '*Propelanomodon*'. J. Vertebr. Paleontol. 36, e1030408.
Kammerer, C.F., Viglietti, P.A., Hancox, P.J., Butler, R.J. and Choiniere, J.N., 2019. A new kannemeyeriiform dicynodont (*Ufudocyclops mukanelai*, gen. et sp. nov.) from Subzone C of the Cynognathus Assemblage Zone, Triassic of South Africa, with implications for biostratigraphic correlation with other African Triassic Faunas. J. Vertebr. Paleontol. 39, e1596921.
Kammerer, C.F., Araújo, R., Cumbane, K., Macungo, Z., Smith, R.M.H. and Angielczyk, K.D., 2022. New material of *Dicynodon angielczyki* (Synapsida: Anomodontia) from Mozambique and

Zambia with biostratigraphic implications for African Permo-Triassic basins. J. Vertebr. Paleontol. 41, e2041652.
Kammerer, C.F., Viglietti, P.A., Butler, E. and Botha, J., 2023. Rapid turnover of top predators in African terrestrial faunas around the Permian-Triassic mass extinction. Curr. Biol. 33, 2283–2290.
Kammerer, C.F., Angielczyk, K.D. and Fröbisch, J., 2025. Permian origins of the Lystrosauridae (Therapsida: Dicynodontia). J. Vertebr. Paleontol. 45(supplement 1), 43–73.
Kemp, T.S., 2005. The Origin and Evolution of Mammals. Oxford University Press, UK.
Keyser, A.W., 1975. A Re-Evaluation of the Cranial Morphology and Systematics of Some Tuskless Anomodontia. Government Printer, Pretoria, South Africa. pp. 1–110.
Keyser, A.W. and Cruickshank, A.R.I., 1979. The origins and classification of Triassic dicynodonts. Trans. Geol. Soc. S. Afr. 82, 81–108.
King, G.M., 1981. The functional anatomy of a Permian dicynodont. Philos. Trans. R. Soc. London-Biol. Sci. 291, 244–322.
King, G.M., 1988. Anomodontia. Gustav Fischer Verlag, Stuttgart.
Kitching, J.W., 1977. The distribution of the Karroo vertebrate fauna. Mem. Bernard Price Inst. Palaeontol. Res. 1, 1–131.
Klein, G.O. (Ed.), 1994. Pangea: Paleoclimate, Tectonics, and Sedimentation During Accretion, Zenith, and Breakup of a Supercontinent. Geological Society of America, USA.
Kurkin, A.A., 2001. New late Permian dicynodonts from the Vyazniki assemblage of terrestrial tetrapods of eastern Europe. Paleontol. J. 35, 53–60.
Lewis, P.O., 2001. A likelihood approach to estimating phylogeny from discrete morphological character data. Syst. Biol. 50, 913–925.
Li, P.-X., Cheng, Z.-W. and Li, J.-L., 2000. A new species of *Dicynodon* from Upper Permian of Sunan, Gansu, with remarks on related strata. Vert. Palasiat. 38, 147–157.
Li, J.-L., Wu, X.-C. and Zhang, F.-C., 2008. The Chinese Fossil Reptiles and Their Kin, second edition. Science Press, China.
Li, S., Huang, Y., Chen, Z.-Q., Chen, L., Wignall, P.B., Dong, J., Liu, X., Zheng, H., Wang, G., Wei, Z. and Zhu, Z., 2024. Variations in antimony isotope and toxic metals across the Guadalupian-Lopingian (Permian) boundary at Penglaitan, China: implications for the Emeishan volcanism and marine extinction. Earth Planet. Sci. Lett. 648, 119096.
Ling, K., Wen, H., Grasby, S.E., Zhao, H., Deng, C. and Yin, R., 2023. The Emeishan large igneous province eruption triggered coastal perturbations and the Capitanian mass extinction: insights from mercury in Permian bauxite beds. Chem. Geol. 617, 121243.
Liu, J., 2020. *Taoheodon baizhijuni*, gen. et sp. nov. (Anomodontia, Dicynodontoidea), from the upper Permian Sunjiagou Formation of China and its implications. J. Vertebr. Paleontol. 40, e1762088.
Liu, J., 2021. The tetrapod fauna of the upper Permian Naobaogou Formation of China: 6. *Turfanodon jiufengensis* sp. nov. (Dicynodontia). PeerJ 9, e10854.
Liu, J., 2022. On kannemeyeriiform dicynodonts from the *Shaanbeikannemeyeria* Assemblage Zone of the Ordos Basin, China. Vert. Palasiat. 60, 212–248.
Liu, J. and Abdala, F., 2022. The emblematic South African therocephalian *Euchambersia* in China: a new link in the dispersal of late Permian vertebrates across Pangea. Biol. Lett. 18, 20220222.
Liu, J. and Abdala, F., 2023. Late Permian terrestrial faunal connections invigorated: the first whaitsioid therocephalian from China. Palaeontol. Afr. 56, 111–117.
Liu, J., Shang, Q.-H., Sun, K.-Q. and Li, L., 2012. The vertebrate fossil-bearing horizon in Yumen, Gansu and the Permian-Triassic strata in north Qilian area. Vert. Palasiat. 50, 373–381.
Liu, J., Angielczyk, K.D. and Abdala, F., 2021. Permo-Triassic tetrapods and their climate implications. Glob. Planet. Chang. 205, 103618.
Liu, J., Abdala, F., Angielczyk, K.D. and Sidor, C.A., 2022. Tetrapod turnover during the Permo-Triassic transition explained by temperature change. Earth Sci. Rev. 224, 103886.
Lucas, S.G., 2009. Timing and magnitude of tetrapod extinctions across the Permo-Triassic boundary. J. Asian Earth Sci. 36, 491–502.
Macungo, Z., Benoit, J., Fernandez, V. and Araújo, R.M.N., 2022. X-ray microcomputed and synchrotron tomographic analysis of the basicranial axis of emydopoid dicynodonts: implications for fossoriality and phylogeny. Zool. J. Linnean Soc. 198, 1–46.
Macungo, Z., Araujo, R., Browning, C., Smith, R., David, R., Angielczyk, K.D., Massingue, A., Ferreira-Cardoso, S. and Kortje, D.J., 2023. Novel anatomy and paleobiological insights on *Cistecephalus microrhinus* (synapsida: dicynodontia). In: Lee, Y.-N. (Ed.), Windows into Sauropsid and Synapsid Evolution: Essays in Honor of Prof. Louis Jacobs. Dinosaur Science Center Press, Hwaseong, South Korea. pp. 1–65.
Macungo, Z., Benoit, J. and Araújo, R., 2025. *Inostrancevia africana*, the first diagnosable gorgonopsian (Therapsida, Synapsida) from the Metangula graben (Mozambique): new anatomical observations and biostratigraphic implications. Swiss J. Palaeontol. 144, 12.
Maharaj, I.E.M., Macungo, Z., Smith, R.M.H., Chinsamy, A. and Araújo, R., 2024. Taxonomic revision of the late Permian dicynodont genus *Endothiodon* (Therapsida, Anomodontia). J. Syst. Palaeontol. 22, 2346578.
Maisch, M.W., 2002. Observations on Karoo and Gondwana vertebrates. Part 4: the taxonomic status of the late Permian rhachiocephalid *Platycyclops crassus* Broom, 1948 (Therapsida: Dicynodontia) from the South African Karoo. Neues Jahrb. Geol. Paläont. 2002, 362–372.
Maisch, M.W., 2005. Observations on Karoo and Gondwana vertebrates. Part 6. A new rhachiocephalid dicynodont (Therapsida) from the Upper Permian of the Ruhuhu Basin (Tanzania). Neues Jahrb. Geol. Paläont. 237, 313–355.
Mallon, J.C. and Anderson, J.S., 2014a. The functional and palaeoecological implications of tooth morphology and wear for the megaherbivorous dinosaurs from the Dinosaur Park Formation (upper Campanian) of Alberta, Canada. PLoS One 9, e98605.
Mallon, J.C. and Anderson, J.S., 2014b. Implications of beak morphology for the evolutionary paleoecology of the megaherbivorous dinosaurs from the Dinosaur Park Formation (upper Campanian) of Alberta, Canada. Palaeogeogr. Palaeoclimatol. Palaeoecol. 394, 29–41.
Matamales-Andreu, R., Kammerer, C.F., Angielczyk, K.D., Simoes, T.R., Mujal, E., Galobart, A. and Fortuny, J., 2024. Early-middle Permian Mediterranean gorgonopsian suggests an equatorial origin of therapsids. Nat. Commun. 15, 10346.
de Mendiburu, F., 2023. Agricolae: statistical procedures for agricultural research. Departamento de Estadistica e Informatica, Universidad Nacional Agraria La Molina, Lima.
Nabavizadeh, A., 2023. How *Triceratops* got its face: an update on the functional evolution of the ceratopsian head. Anat. Rec. 306, 1951–1968.
Olivier, C., Battail, B., Bourquin, S., Rossignol, C., Steyer, J.S. and Jalil, N.-E., 2019. New dicynodonts (Therapsida, Anomodontia) from near the Permo-Triassic boundary of Laos: implications for dicynodont survivorship across the Permo-Triassic mass extinction and the paleobiogeography of Southeast Asian blocks. J. Vertebr. Paleontol. 39, e1584745.
Olroyd, S.L. and Sidor, C.A., 2017. A review of the Guadalupian (middle Permian) global tetrapod fossil record. Earth Sci. Rev. 171, 583–597.
Pimentel, R.A. and Riggins, R., 1987. The nature of cladistic data. Cladistics 3, 201–209.
R Core Team, 2024. R: A Language and Environment for Statistical Computing. R Foundation for Statistical Computing, Vienna.
Rae, T.C., 1998. The logical basis for the use of continuous characters in phylogenetic systematics. Cladistics 14, 221–228.
Rambaut, A., Drummond, A.J., Xie, D., Baele, G. and Suchard, M.A., 2018. Posterior summarization in Bayesian phylogenetics using Tracer 1.7. Syst. Biol. 67, 901–904.

Ray, S., 2000. Endothiodont dicynodonts from the late Permian Kundaram formation, India. Palaeontology 43, 375–404.
Rees, P.M., Ziegler, A.M., Gibbs, M.T., Kutzbach, J.E., Behling, P.J. and Rowley, D.B., 2002. Permian phytogeographic patterns and climate data/model comparisons. J. Geol. 110, 1–31.
Ronquist, F., Teslenko, M., van der Mark, P., Ayres, D.L., Darling, A., Hohna, S., Larget, B., Liu, L., Suchard, M.A. and Huelsenbeck, J.P., 2012. MrBayes 3.2: efficient Bayesian phylogenetic inference and model choice across a large model space. Syst. Biol. 61, 539–542.
Roscher, M. and Schneider, J.W., 2006. Permo-Carboniferous climate: early Pennsylvanian to late Permian climate development of central Europe in a regional and global context. In: Lucas, S.G., Cassinis, G. and Schneider, J.W. (Eds.), Non-Marine Permian Biostratigraphy and Biochronology. Geological Society of London Special Publication, London, UK. pp. 95–136.
Roscher, M., Stordal, F. and Svensen, H., 2011. The effect of global warming and global cooling on the distribution of the latest Permian climate zones. Palaeogeogr. Palaeoclimatol. Palaeoecol. 309, 186–200.
Rowe, T., 1980. The morphology, affinities, and age of the dicynodont reptile *Geikia elginensis*. In: Jacobs, L.L. (Ed.), Aspects of Vertebrate History. Museum of Northern Arizona Press, Flagstaff, USA. pp. 269–294.
Rubidge, B.S., Erwin, D.H., Ramezani, J., Bowring, S.A. and de Klerk, W.J., 2013. High-precision temporal calibration of late Permian vertebrate biostratigraphy: U-Pb zircon constraints from the Karoo Supergroup, South Africa. Geology 41, 363–366.
Saguir, S.O., Haidr, N.S., Flores, D.A. and Catalano, S.A., 2025. Phylogenetic analysis of geometric morphometric data: a study case in Didelphidae. Zool. Scr. 54, 437–453.
Schneider, J.W., Körner, F., Roscher, M. and Kroner, U., 2006. Permian climate development in the northern peri-Tethys area – the Lodève basin, French Massif Central, compared in a European and global context. Palaeogeogr. Palaeoclimatol. Palaeoecol. 240, 161–183.
Scotese, C.R., Vérard, C., Burgener, L., Elling, R.P. and Kocsis, A.T., 2025. The Cretaceous world: plate tectonics, palaeogeography and palaeoclimate. In: Hart, M.B., Batenburg, S.J., Huber, B.T., Price, G.D., Thibault, N., Wagreich, M., Walaszczyk, I. (Eds.), Cretaceous Project 200 Volume 1: the Cretaceous World. Geological Society of London, London, UK. pp. 31–202.
Sennikov, A.G. and Golubev, V.K., 2017. Sequence of Permian tetrapod Faunas of Eastern Europe and the Permian–Triassic ecological crisis. Paleontol. J. 51, 600–611.
Shi, Y.-T. and Liu, J., 2023. The tetrapod fauna of the upper Permian Naobaogou Formation of China: 10. *Jimusaria monanensis* sp. nov. (Dicynodontia) shows a unique epipterygoid. PeerJ 11, e15783.
Shi, Y.-T. and Liu, J., 2024. Osteology of *Turfanodon bogdaensis* (Dicynodontia). Vert. Palasiat. 62, 186–200.
Shishkin, M.A., Novikov, I.V., Sennikov, A.G., Golubev, V.K. and Morkovin, B.I., 2024. Chapter I. Annotated systematic catalog of Triassic tetrapods of Russia. Paleontol. J. 57, 1363–1468.
Simões, T.R., Kammerer, C.F., Caldwell, M.W. and Pierce, S.E., 2022. Successive climate crises in the deep past drove the early evolution and radiation of reptiles. Sci. Adv. 8, eabq1898.
Simon, C., 1983. A new coding procedure for morphometric data with an example from periodical cicada wing veins. In: Felsenstein, J. (Ed.), Numerical Taxonomy. Springer Berlin Heidelberg, Berlin, Heidelberg, Germany. pp. 378–382.
Smith, R.M.H., 2020. Biostratigraphy of the *Cistecephalus* Assemblage Zone (Beaufort Group, Karoo Supergroup), South Africa. S. Afr. J. Geol. 123, 181–190.
Smith, R.M.H., Sidor, C.A., Tabor, N.J. and Steyer, J.S., 2015. Sedimentology and vertebrate taphonomy of the Moradi Formation of northern Niger: a Permian wet desert in the tropics of Pangaea. Palaeogeogr. Palaeoclimatol. Palaeoecol. 440, 128–141.
Smith, R.M.H., Rubidge, B.S., Day, M.O. and Botha, J., 2020. Introduction to the tetrapod biozonation of the Karoo Supergroup. S. Afr. J. Geol. 123, 131–140.
Stadler, T., 2010. Sampling-through-time in birth–death trees. J. Theor. Biol. 267, 396–404.
Sullivan, C. and Reisz, R.R., 2005. Cranial anatomy and taxonomy of the late Permian dicynodont *Diictodon*. Ann. Carnegie Museum 74, 45–75.
Sun, A.-L., 1973. Permo-Triassic dicynodonts from Turfan, Sinkiang. Mem. Inst. Vert. Paleontol. Paleoanthropol., Acad. Sin. 10, 53–68.
Surkov, M.V., Kalandadze, N.N. and Benton, M.J., 2005. *Lystrosaurus georgi*, a dicynodont from the Lower Triassic of Russia. J. Vertebr. Paleontol. 25, 402–413.
Szczygielski, T. and Sulej, T., 2023. *Woznikella triradiata* n. gen., n. sp. – a new kannemeyeriiform dicynodont from the Late Triassic of northern Pangea and the global distribution of Triassic dicynodonts. C. R. Palevol. 22, 279–406.
Tabor, N.J., Smith, R.M.H., Steyer, J.S., Sidor, C.A. and Poulsen, C.J., 2011. The Permian Moradi Formation of northern Niger: paleosol morphology, petrography and mineralogy. Palaeogeogr. Palaeoclimatol. Palaeoecol. 299, 200–213.
Tagliacollo, V.A., de Pinna, M., Chuctaya, J. and Datovo, A., 2025. Accuracy of phylogenetic reconstructions from continuous characters analysed under parsimony and its parametric correlates. Cladistics 41, 212–222.
Tsuji, L.A., Sidor, C.A., Steyer, J.S., Smith, R.M.H., Tabor, N.J. and Ide, O., 2013. The vertebrate fauna of the Upper Permian of Niger—VII. Cranial anatomy and relationships of *Bunostegos akokanensis* (Pareiasauria). J. Vertebr. Paleontol. 33, 747–763.
Viaretti, M., Crippa, G., Brombin, V., Della Porta, G., Griesshaber, E., Jurikova, H., Posenato, R., Bottini, C. and Angiolini, L., 2025. Duration and intensity of the late Permian (early Wuchiapingian) cool climate episode: Sclerochemical evidence from brachiopod assemblages in Iran. Palaeogeogr. Palaeoclimatol. Palaeoecol. 659, 112654.
Viglietti, P.A., 2020. Biostratigraphy of the *Daptocephalus* assemblage zone (Beaufort Group, Karoo Supergroup), South Africa. S. Afr. J. Geol. 123, 191–206.
Viglietti, P.A., Benson, R.B.J., Smith, R.M.H., Botha, J., Kammerer, C.F., Skosan, Z., Butler, E., Crean, A., Eloff, B., Kaal, S., Mohoi, J., Molehe, W., Mtalana, N., Mtungata, S., Ntheri, N., Ntsala, T., Nyaphuli, J., October, P., Skinner, G., Strong, M., Stummer, H., Wolvaardt, F.P. and Angielczyk, K.D., 2021. Evidence from South Africa for a protracted end-Permian extinction on land. Proc. Natl. Acad. Sci. USA 118, e2017045118.
Voigt, S., Hminna, A., Saber, H., Schneider, J.W. and Klein, H., 2010. Tetrapod footprints from the uppermost level of the Permian Ikakern formation (Argana Basin, western high Atlas, Morocco). J. Afr. Earth Sci. 57, 470–478.
Wang, W.-q., Garbelli, C., Zhang, F.-f., Zheng, Q.-f., Zhang, Y.-c., Yuan, D.-x., Shi, Y.-k., Chen, B. and Shen, S.-z., 2020. A high-resolution Middle to late Permian paleotemperature curve reconstructed using oxygen isotopes of well-preserved brachiopod shells. Earth Planet. Sci. Lett. 540, 116245.
Wignall, P.B., Sun, Y., Bond, D.P.G., Izon, G., Newton, R.J., Védrine, S., Widdowson, M., Ali, J.R., Lai, X., Jiang, H., Cope, H. and Bottrell, S.H., 2009. Volcanism, mass extinction, and carbon isotope fluctuations in the Middle Permian of China. Science 324, 1179–1182.
Yang, W., Wan, M., Crowley, J.L., Wang, J., Luo, X., Tabor, N., Angielczyk, K.D., Gastaldo, R., Geissman, J., Liu, F., Roopnarine, P. and Sidor, C.A., 2021. Paleoenvironmental and paleoclimatic evolution and cyclo- and chrono-stratigraphy of upper Permian–Lower Triassic fluvial-lacustrine deposits in Bogda Mountains, NW China – implications for diachronous plant evolution across the Permian–Triassic boundary. Earth Sci. Rev. 222, 103741.
Yuan, P.L. and Young, C.C., 1934. On the occurrence of *Lystrosaurus* in sinkiang. Bull. Geol. Surv. China 13, 575–580.

Zhang, C., Stadler, T., Klopfstein, S., Heath, T.A. and Ronquist, F., 2016. Total-evidence dating under the fossilized birth–death process. Syst. Biol. 65, 228–249.

Supporting Information

Additional supporting information may be found online in the Supporting Information section at the end of the article.

Fig. S1. The synapomorphies of the strict consensus parsimonious tree.

Fig. S2. The initial results of the tip-dating analysis without constraints. Note that the inferred divergence times of Kingoriidae, *Emydops*, *Endothiodon*, *Dinanomodon*, Rhachiocephalidae, and some geikiids are younger than their first appearance datum (FAD). All ages were subtracted 230 Ma.

Appendix S1. The commands for MrBayes.

Appendix S2. Phylogeny data set.

Data S1. Character matrix for phylogenetic analyses.

Data S2. Specimen measurements of coded dicynodonts.